Paleomagnetism and tectonics of the southern Atacama Desert (25–28°S), northern Chile

César Arriagada,[1] Pierrick Roperch,[2,3] Constantino Mpodozis,[4,5] and Rodrigo Fernandez[1]

Received 9 November 2005; revised 14 March 2006; accepted 29 March 2006; published 1 July 2006.

[1] We report paleomagnetic results for 131 sites from the modern forearc of northern Chile (25°S and 28°S). Remanent magnetization in volcanic and intrusive rocks is mostly primary, while a secondary magnetization is observed in sedimentary rocks. Comparison of locality-mean directions with expected paleomagnetic directions indicates vertical axis rotations from $-7.3° \pm 21.6°$ counterclockwise to $52.7° \pm 17°$ clockwise. Jurassic to Early Cretaceous rocks from the Coastal Cordillera and Cretaceous to Paleocene rocks from the Central Depression show similar magnitude (>30°) clockwise rotations, while more variable rotations occur in Mesozoic to Eocene rocks of the Precordillera. Clockwise rotations in Mesozoic and Paleogene rocks occur in the Chilean Frontal Cordillera south of 27°30′S. Paleomagnetic results in three large Miocene ignimbrite sheets overlying rotated and nonrotated older rocks in the Precordillera and Pre-Andean Depression which show no relative rotation between sites indicate that most rotations within the study area occurred prior to 18 Ma (early Miocene) and likely during and after the ''Incaic'' tectonic event, which affected large tracts of the central Andes. The postulated onset of rotations in the north Chilean forearc was contemporaneous with the beginning of horizontal shortening and uplift of the Eastern Cordillera in Bolivia and northwestern Argentina. Rotation of the Chilean forearc, enhancement of the curvature of the central Andes, and the formation of the Bolivian Orocline seem to be, for the most part, closely linked to the evolution of the Eocene-Oligocene tectonics of the Eastern Cordillera.
Citation: Arriagada, C., P. Roperch, C. Mpodozis, and R. Fernandez (2006), Paleomagnetism and tectonics of the southern Atacama Desert (25–28°S), northern Chile, *Tectonics*, *25*, TC4001, doi:10.1029/2005TC001923.

1. Introduction

[2] Paleomagnetically determined vertical axis block rotations are an important component of deformation in the central Andes [*Macedo Sanchez et al.*, 1992; *Butler et al.*, 1995; *MacFadden et al.*, 1995; *Randall et al.*, 1996, 2001; *Aubry et al.*, 1996; *Somoza et al.*, 1999; *Coutand et al.*, 1999; *Roperch et al.*, 2000; *Arriagada et al.*, 2000, 2003; *Somoza and Tomlinson*, 2002]. Rotations are systematically counterclockwise in southern Peru and clockwise in northern Chile. Although some workers consider that this pattern is controlled by differences in the magnitude of Neogene shortening along the Sub-Andean Fold and Thrust Belt, which finally led to the formation of the Arica Bend and the Bolivian Orocline [i.e., *Isacks*, 1988] most of the available paleomagnetic data indicate amounts of rotation whose magnitudes exceed those predicted by Isacks' model. The greatest discrepancies occur in northern Chile where clockwise rotations larger than 40° have been documented [see *Randall et al.*, 1996; *Arriagada et al.*, 2000, 2003, and reference therein]. Such large rotations have been found in Mesozoic and Paleocene rocks in the Central Depression (Central Valley) and Precordillera near Antofagasta [*Arriagada et al.*, 2003] and Mesozoic volcanic rocks and coeval Jurassic to late Early Cretaceous arc plutons in the Coastal Cordillera between Taltal and Chañaral [*Forsythe and Chisholm*, 1994; *Randall et al.*, 1996].

[3] The timing, origin and this ''excess rotation'' are unclear. *Randall et al.* [1996] and *Taylor et al.* [1998] hypothesize that clockwise rotations in the Coastal Cordillera between Taltal and Copiapó (25–28°S, Figure 1) can be explained by local ''domino style'' deformation associated to mid or late Cretaceous sinistral transpression. However, clockwise rotations of similar magnitude have been also found, farther east, in Late Cretaceous–Paleocene sequences on the Central Depression and Cordillera de Domeyko, in Antofagasta (22–23°S [*Arriagada et al.*, 2003]) and Copiapó (26–28°S, Figure 1 [*Riley et al.*, 1993; *Randall et al.*, 2001; *Taylor et al.*, 2002]) which indicate that local-scale processes cannot totally explain these tectonic rotations. While Paleocene volcanics in Antofagasta and Copiapó are rotated, Miocene ignimbrites, outcropping in the Precordillera of Antofagasta, show no evidences of rotation [*Somoza et al.*, 1999; *Somoza and Tomlinson*, 2002]. This observation led *Arriagada et al.* [2003] to suggest that most of the rotations occurred during the Paleogene, possibly in conjunction with the late Eocene–early Oligocene Incaic tectonic event which affected large areas of northern

[1]Departamento de Geología, Universidad de Chile, Santiago, Chile.
[2]Departamento de Geología, Universidad de Chile, Institut de Recherche pour le Développement, Santiago, Chile.
[3]Now at Institut de Recherche pour le Développement, UR154, Géosciences-Rennes, Université de Rennes 1, Rennes, France.
[4]Servicio Nacional de Geología y Minería, Santiago, Chile.
[5]Now at ENAP-Sipetrol, Santiago, Chile.

0278-7407/06/2005TC001923

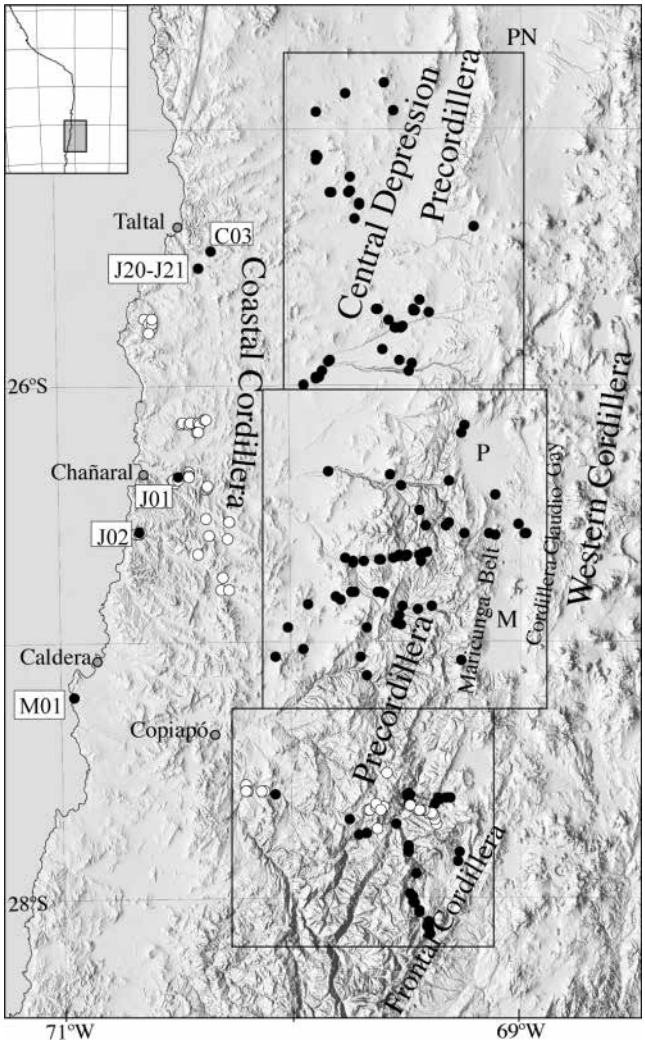

Figure 1. Simplified sketch of the forearc of northern Chile and location of paleomagnetic sampling. Rectangles indicate the location of the maps shown in Figures 2a, 2b, and 2c. Solid circles are paleomagnetic sites from this study. Open circles are paleomagnetic sites from *Riley et al.* [1993] and *Randall et al.* [1996]. PN, Punta Negra; P, Pedernales; M, Maricunga.

Chile and produced tectonic shortening, transpression, uplift and erosion in the Cordillera de Domeyko [see *Tomlinson et al.*, 1993; *Maksaev and Zentilli*, 1999; *Müller et al.*, 2002; *Muñoz et al.*, 2005] during a period of fast oblique convergence between the Farallon and South American plates [*Pardo-Casas and Molnar*, 1987].

[4] In this contribution we present the results of a large-scale paleomagnetic study during which more than 1000 samples were collected from the Coastal Cordillera to the Pre-Andean Depression of the southern Atacama Desert between 25°S and 28°S (Figure 1). These new data, which are consistent with the results we have already obtained farther north, are utilized to propose a new tectonic model to explain the origin of the rotations and the geodynamic evolution of this key region of the central Andes.

2. Geological and Tectonic Setting of the Chilean Andes Between 24 and 28°S

[5] The southern Atacama Desert region (24–28°S, Figures 1 and 2a–2c) is located on the gentle tectonic transition zone between the steeply dipping subducting slab segment of northern Chile and the "Pampean" flat slab segment of central Chile and Argentina [*Cahill and Isacks*, 1992]. Morphological units in the present-day forearc comprise the Coastal Cordillera, Central Depression and the Cordillera de Domeyko (or "Precordillera"). In the studied region, from 26° to 28°S the Cordillera de Domeyko also includes a string of mildly eroded volcanic centers which are the remnants of the extinct Oligocene-Miocene Andean volcanic front (Maricunga belt [*Mpodozis et al.*, 1995]). Forty kilometers to the east the Neogene-Quaternary arc volcanoes of the Western Cordillera, rising more than 6 km above sea level, form the international boundary with Argentina. The "Pre-Andean Depression", hosting the Punta Negra, Pedernales, and Maricunga basins, fills the gap between the two volcanic lines (Figures 1 and Figures 2a–2c). South of 27°40′S the Pre-Andean Depression terminates and the Cordillera de Domeyko merges with the basement cored block uplifts of the Frontal Cordillera which from there on form the international boundary with Argentina.

2.1. Coastal Cordillera and Central Depression

[6] The oldest rocks cropping out in the Costal Cordillera are low-grade Devonian(?) to Carboniferous low-grade metasediments, and Permian-Triassic plutonic complexes which are uncomformably covered by late Triassic to early Jurassic, sedimentary sequences accumulated in restricted extensional basins [*Naranjo and Puig*, 1984; *Grocott and Taylor*, 2002] (Figure 1). Yet, the most important components of the Coastal Cordillera are the magmatic products of the early (Jurassic–early Cretaceous) Andean arcs, including thick successions of tholeithic to calc-alkaline basaltic to dacitic lavas and domes (La Negra Formation and Punta del Cobre Group [*Godoy and Lara*, 1998; *Matthews et al.*, 2006]) which, south of 26°30′S, are capped by up to 2000 m of early Cretaceous marine limestones (Chañarcillo Group [*Arévalo*, 1999]). These Mesozoic volcanic rocks and limestones are intruded by the eastward younging plutons of the Coastal Batholith, whose K/Ar, Ar/Ar and U/Pb ages peak at 190–180, 150–140, 120–130, and 110–90 Ma [*Dallmeyer et al.*, 1996]. Ductile to brittle faults along the arc axis, collectively described in the literature as the Atacama Fault System, record alternating events of extension and/or left-lateral strike slip to transtensional intra-arc deformation during Jurassic and early Cretaceous times. A major extensional (transtensional?) episode occurred during the mid-Cretaceous (110–90 Ma) at which time shallow angle detachments faults exhumed Paleozoic basement in parts of the Central Depression and Precordillera [*Mpodozis and Allmendinger*, 1993] and thick sequences of coarse

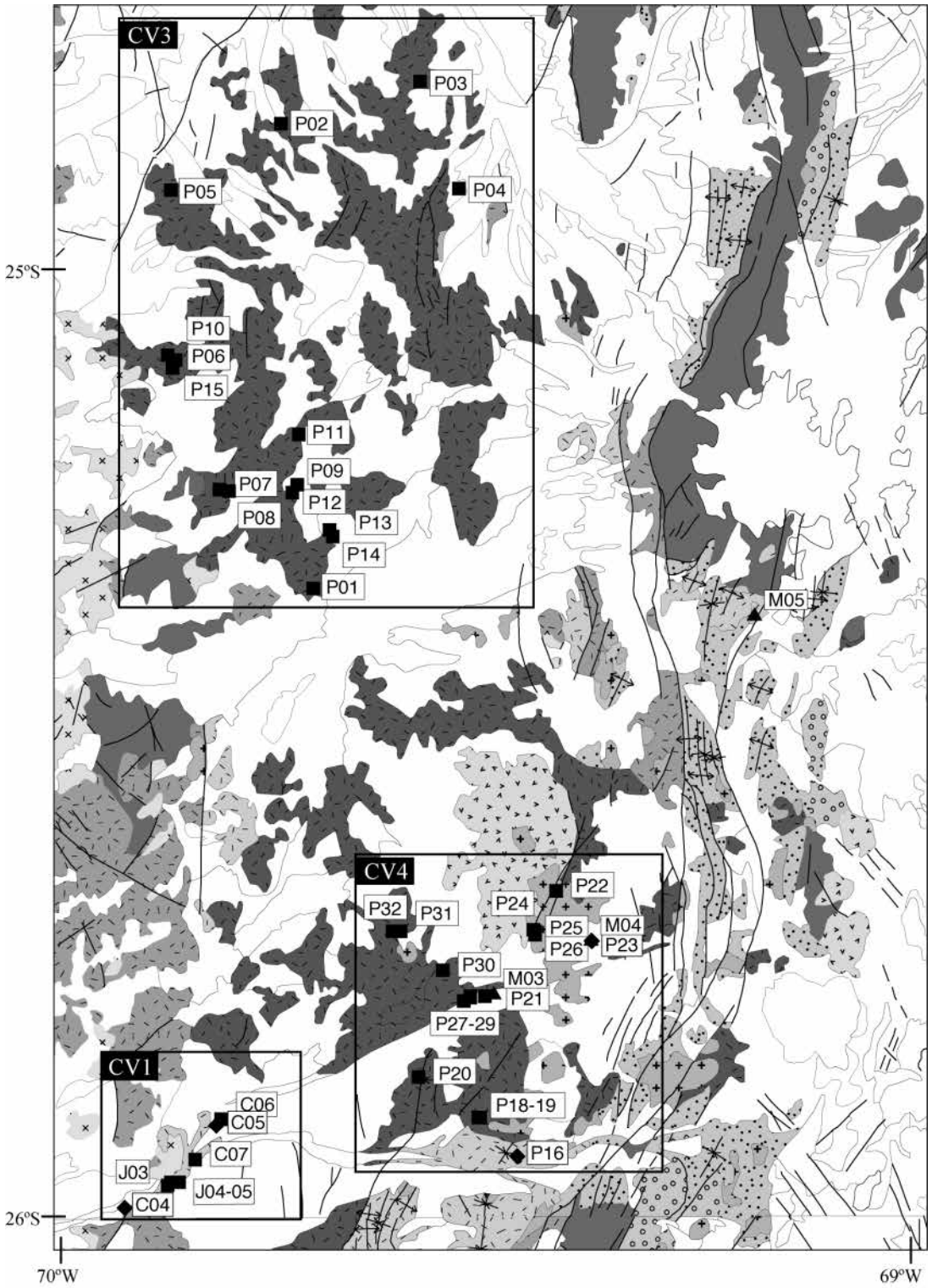

Figure 2a. Geological map of the Atacama region showing paleomagnetic sites (modified after *Servicio Nacional de Geología y Minería* [2003]). Paleomagnetic sites are shown by solid squares (volcanic rocks), diamonds (intrusive), triangles (Neogene ignimbrites), and circles (sediments). The letters M, O, E, P, C, and J before the site number correspond to the age of sampled unit (M, Miocene; O, Oligocene; E, Eocene; P, Paleocene; C, Cretaceous; J, Jurassic). CV1, CV3, CV4 correspond to localities in the Central Valley. Legend is the same as in Figure 2c.

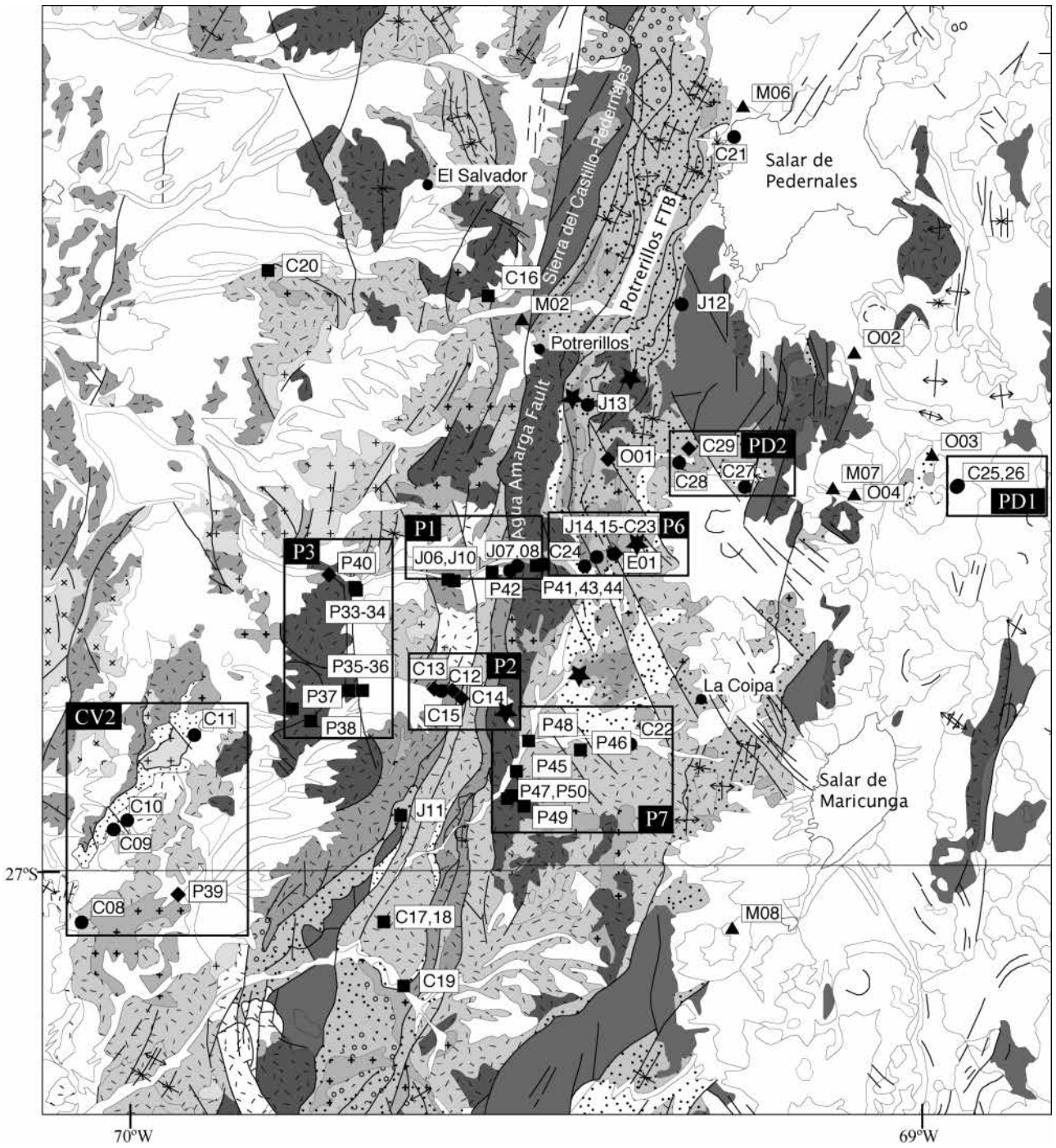

Figure 2b. Paleomagnetic sampling and localities in the Precordillera (P) and the Pre-Andean Depression (PD). Solid stars correspond to localities from *Randall et al.* [2001]. Legend is the same as in Figure 2c.

grained terrestrial sediments and volcanoclastic breccias (Cerrillos Formation [*Arévalo*, 1999]) accumulated in coeval extensional basins along the eastern border of the Coastal Cordillera. After a first compressional episode which affected the whole Andean domain in the earliest late Cretaceous, at circa 85 Ma [*Mpodozis and Ramos*, 1990; *Mpodozis et al.*, 2005] the magmatic front migrated eastward toward the Central Valley (Figures 1 and Figures 2a–2c) where unconsolidated Neogene sediments partially, conceals a series of fault-bounded transtensional(?) basins filled by thick successions of latest Cretaceous (85–64 Ma) sediments, basic lavas and ignim-

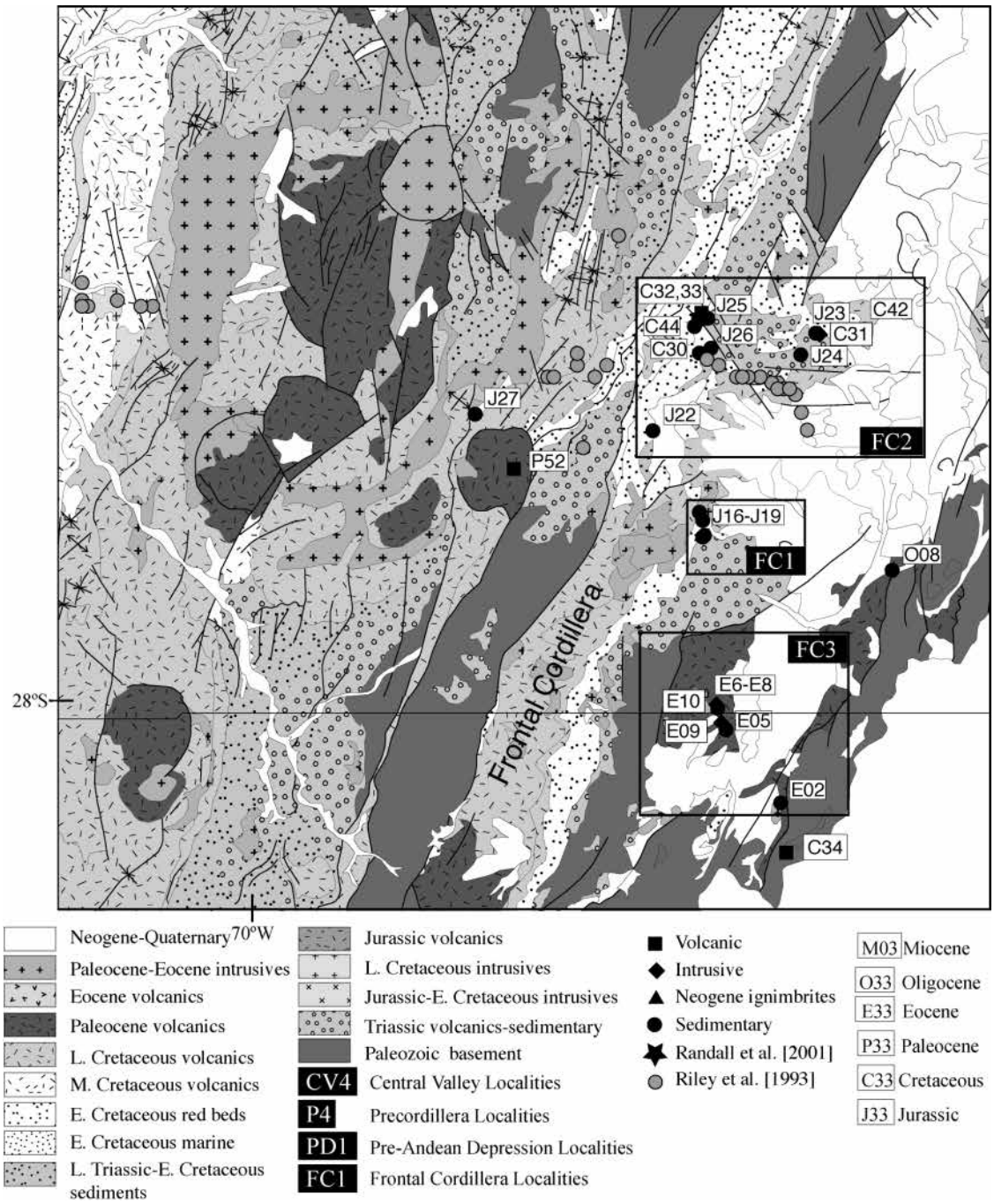

Figure 2c. Paleomagnetic sampling and localities in the Frontal Cordillera (FC). Grey circles correspond to sampling sites from *Riley et al.* [1993].

brites ("Hornitos" sequence and equivalents [*Arévalo et al.*, 1994; *Cornejo and Mpodozis*, 1996]). These late Cretaceous strata are covered by a string of Paleocene-Eocene volcanic complexes, which include rhyolitic domes, some deeply eroded andesitic stratovolcanoes and numerous collapse calderas which erupted after a major compressive deformation event which took place around the Cretaceous-Tertiary boundary [*Cornejo et al.*, 1993] (Figures 2a–2c).

2.2. Cordillera de Domeyko (Precordillera)

[7] The oldest rocks exposed in the Precordillera (Figures 1 and Figures 2a–2c) are Devonian-Carboniferous sediments and Permian volcanics intruded by Permian batholiths and, as in the Coastal Cordillera, covered by alluvial/fluvial, lacustrine and siliclastic marine and bimodal (alkaline basalt-rhyolite) volcanic suites deposited in rift basins during the late Triassic–earliest Jurassic [*Cornejo et*

al., 1993; *Cornejo and Mpodozis*, 1996]. Thick sequences of shallow water, marine carbonates, which interfinger to the west with the distal volcanic products of the Coastal Cordillera arc, accumulated in a back arc basin setting (Tarapacá back-arc basin) during the Jurassic–earliest Cretaceous [*Cornejo et al.*, 1993; *Cornejo and Mpodozis*, 1996]. Marine conditions ended in the Precordillera in the early Cretaceous when continental (fluvial/eolian sandstones) accumulated along the whole back-arc domain (i.e., Quebrada Monardes Formation). Late Cretaceous and Paleocene–early Eocene volcanic units were deposited after back arc basin inversion in the late Cretaceous [*Cornejo et al.*, 1993].

[8] The Precordillera is a complex structural domain shaped by successive deformation increments on the Domeyko Fault System (DFS), a major longitudinal belt of deformation, which extends for more than 800 km along the Precordillera axis from Iquique (19°S) to Copiapó (27°) [*Maksaev and Zentilli*, 1999]. The ~40 km wide DFS include structures formed during Jurassic extension, late Cretaceous basin inversion and earliest Cenozoic compression reactivated and overprinted during the mid-Eocene–early Oligocene (45–35 Ma) ''Incaic'' tectonic event [*Cornejo et al.*, 1993]. Subvolcanic stocks and porphyries, were emplaced along the major DFS fault strands during the Eocene–early Oligocene (45–35 Ma [*Cornejo et al.*, 1993; *Cornejo and Mpodozis*, 1996]). Evidences of important exhumation and uplift of the Precordillera during the Incaic event comes from apatite fission track data presented by *Maksaev and Zentilli* [1999] and *Nalpas et al.* [2005] while geochemical evidences for contemporaneous crustal thickening has been shown by *Cornejo et al.* [1999] and *Cornejo and Matthews* [2000].

[9] DFS structures include thick-skinned basement blocks uplifts (Sierra del Castillo-Pedernales, Figures 2a–2c), thin-skinned fold and thrust belts such as the one near Potrerillos (Figures 2a–2c) and left-lateral strike-slip faults including the NW trending faults of the Potrerillos–La Coipa structural corridor [*Tomlinson et al.*, 1993] (Figures 2a–2c). South of 27°30′S, basement cored anticlines formed during the Incaic event are dissected by early(?) Miocene high-angle N-S to NNE reverse faults attaining several kilometers of vertical throw which farther south dominate the structural fabric of the Frontal Cordillera (Figures 2a–2c) in the Pampean flat slab region [*Moscoso and Mpodozis*, 1988].

2.3. Pre-Andean Depression

[10] From 22° to 27°S, the Pre-Andean Depression includes a series of closed basins, which besides hosting the active Punta Negra, Pedernales and Maricunga salars (saline playa lakes) are filled with thick late Cretaceous to Neogene continental clastic sequences. Fill units of the Pedernales basin contain late Cretaceous synorogenic continental clastic strata and minor volcanic rocks (Leoncito Formation) and a continental strata of probably Paleocene age which accumulated in a foreland basin setting after the early late Cretaceous inversion of the Mesozoic back-arc basin [*Cornejo et al.*, 1993; *Mpodozis and Clavero*, 2002]. Eocene–early Oligocene epiclastic and pyroclastic units directly overlie Permian intrusives and volcanics at Cordillera Claudio Gay, to the east of the Pedernales and Maricunga basins (Figures 2a–2c) where evaporite-rich continental red beds, which also has been recognized south of 27°S, were deposited during the Oligocene [*Mpodozis et al.*, 1995; *Mpodozis and Clavero*, 2002]. After inception of Maricunga arc volcanism along the axis of eastern edge of the Precordillera at 26 Ma, coarse proximal pyroclastic and volcanoclastic sediments and back arc basalts (Segerstrom Basalts [*Kay et al.*, 1991]) were deposited in both the Pedernales and Maricunga basins during the late Oligocene–early Miocene before high-angle reverse faults uplifted the Cordillera Claudio Gay at around 21–20 Ma. Dome complexes associated with extensive block-and-ash flow aprons were emplaced along the northern part of Cordillera Claudio Gay at 20–19 Ma to be shortly thereafter covered by a widespread dacitic ignimbrite sheet (Vega Helada Ignimbrite, 18–19 Ma) which probably originated during the volcanic collapse related to the formation of the giant Aguilar Caldera at 26°S which was also the source of the huge ignimbrite sheets (Rio Frío Ignimbrite) which cover a large plateau south of Salar de Punta Negra [*Cornejo and Mpodozis*, 1996]. Finally, during the middle Miocene the Pedernales-Maricunga Basin experienced a last pulse of compressional deformation, which affected particularly the area east of the presently active basins as indicated by the accumulation of alluvial gravels interbedded with distal ignimbrite sheets (15–16 Ma, K/Ar). These show progressive unconformities and intraformational folds, indicative of synsedimentary deformation [*Mpodozis and Clavero*, 2002].

3. Paleomagnetism

3.1. Sampling

[11] Paleomagnetic sampling was carried out on the course of several field seasons during which we collected more than 1000 oriented cores [*Fernández*, 2003]. Here we report results from the Coastal Cordillera (6 sites), Central Depression (45 sites), Precordillera (43 sites), Pre-Andean Depression (11 sites) and the Frontal Cordillera south of 27°30′S (26 sites) (auxiliary material[1], Table 1, and Figures 1 and Figures 2a–2c). Most of the sampling was carried out with a portable gasoline-powered drill system, and samples were oriented using magnetic and solar compasses whenever possible.

3.2. Paleomagnetic Techniques

[12] Remanent magnetization was measured with spinner magnetometers (Molspin or AGICO JR5A) while magnetic susceptibility was measured with a Bartington susceptibility meter at the Laboratory of Paleomagnetism, Geology Department, Universidad de Chile, in Santiago. To better constrain the magnetic mineralogy, we analyzed the acqui-

[1] Auxiliary material is available at ftp://ftp.agu.org/apend/tc/2005tc001923.

Table 1. Paleomagnetic Data and Results[a]

Site	Lithology	S/D	N/n/p	In Situ Dec	In Situ Inc	α95	k	Tilt Corrected Dec	Tilt Corrected Inc	Type	Age
Coastal Cordillera Domain: Locality CC1, Jurassic Dikes near Chañaral											
J01	Vetado	0/0	6/6/0	46.1	−55.4	7.5	80	46.1	−55.4	A	LJ
J02	Flamenco	0/0	7/7/0	234.2	51.8	6.6	84	234.2	51.8	A	LJ
J02	Flamenco	0/0	6/6/0	57.2	−42.6	9.0	56	57.2	−42.6	B	LJ
Coastal Cordillera Domain: Late Miocene (Caldera Formation)											
M01	siltstones	0/0	5/5/0	351.6	−38.5	**4.4**	**299**	**351.6**	**−38.5**	A	LM
Central Valley Domain: Locality CC2, Late Jurassic-Early Cretaceous (La Negra Fm.) and Early Cretaceous (Intrusive)											
J20	lava flow	51/10	10/10/0	225.3	59.3	2.2	467	209.6	56.9	A	EC
J21	lava flow	209/10	9/9/0	18.0	−37.4	3.1	276	25.8	−38.7	A	EC
C03	intrusive	0/0	10/5/5	178.4	49.4	4.5	126	178.4	49.4	A	EC
Central Valley Domain: Locality CV1a, Late Jurassic-Early Cretaceous (La Negra Fm.)											
J03	lava flow	131/25	11/10/1	187.2	47.1	6.3	54	196.3	25.2	A	EC
J04	lava flow	128/27	11/11/0	193.1	55.2	4.3	114	201.9	29.7	A	EC
J05	lava flow	136/23	10/4/6	181.1	69.7	7.2	50	203.9	49.7	A	EC
Mean IS CC2 + CV1a			13.6	−53.9	12.2	31					
Mean TC CC2 + CV1a						**12.3**	**30**	**19.2**	**−42.1**		
Central Valley Domain: Locality CV1b, Late Cretaceous (Llanta Formation)											
C04	stock	188/14	12/12/0	40.3	−69.4	3.3	172	61.5	−60.1	A	LC
C05	dike	141/5	9/7/0	175.6	53.0	4.2	210	180.6	49.9	A	LC
C06	lava flow	141/5	8/3/5	35.9	−36.9	3.7	275	36.7	−32.1	A	LC
C06[b]	lava flow	141/5	7/4/3	202.5	54.2	4.2	235	205.4	49.8	B/C	LC
C07	lava flow	106/5	8/8/0	33.3	−43.5	8.5	43	32.0	−38.7	A	LC
Mean IS				205.5	52.4	15.7	25				
Mean TC						**16.8**	**22**	**210.3**	**47.5**		
Central Valley Domain: Locality CV2, Early Cretaceous (Chañarcillo Group) and Late Cretaceous-Paleocene Intrusive (South of Inca de Oro Area)											
C08	sandstones	15/26	13/13/0	204.5	60.4	3.2	173	162.6	54.8	B/C	LC/Pal
C09	limestones	69/73	5/4/1	68.4	−69.6	9.7	72	0.6	−15.3	B	LC/Pal
C10	sandstones	85/57	8/8/0	92.3	−65.2	7.6	54	24.6	−33.0	B	LC/Pal
C11[c]	limestones	121/11	12/12/0	203.5	59.4	7.4	35			B	
C11[c]	limestones		12/12/0			4.9	79	204.6	47.7	B	LC/Pal
P39	monzodiorite	0/0	6/0/6	230.0	65.8	1.7	2526	230.0	65.8	A	Pal
Mean IS				48.6	−66.5	12.6	37				
Mean TC						24.9	10	13.8	−45.6		
Stepwise	**25**%					**9.4**	**67**	**34.3**	**−63.0**		
Central Valley Domain: Locality CV3, Paleocene (Catalina-Aguas Blancas Region)											
P01	lava flow	343/24	11/11/0	210.2	37.6	4.4	107	190.4	52.9	A	Pal
P02[b]	ignimbrite	0/0	12/12/0	287.6	69.9	4.4	99	287.6	69.9	A	Pal
P03	lava flow	0/0	12/5/7	209.9	51.3	3.9	132	209.9	51.3	A	Pal
P04	lava flow	219/13	7/2/5	173.4	51.7	4.2	274	189.3	60.1	A	Pal
P05	lava flow	219/13	11/11/0	211.3	38.1	1.7	763	222.3	38.5	A	Pal
P06[c]	ignimbrite	0/0	8/6/2	35.0	−50.3	1.5	1490	35.0	−50.3	A	Pal
P07	ignimbrite	0/0	11/11/0	207.4	35.1	2.9	259	207.4	35.1	A	Pal
P08	lava flow	0/0	11/9/2	200.9	52.4	3.1	227	200.9	52.4	A	Pal
P09	ignimbrite	0/0	8/8/0	48.3	−68.4	2.9	360	48.3	−68.4	A	Pal
P10	ignimbrite	0/0	10/10/0	218.3	45.1	2.1	530	218.3	45.1	A	Pal
P11	lava flow	0/0	9/6/3	198.7	68.9	5.5	93	198.7	68.9	A	Pal
P12	lava flow	0/0	7/3/4	219.5	27.4	8.2	62	219.5	27.4	A	Pal
P13[b]	ignimbrite	0/0	8/8/0	195.7	−2.6	2.6	448	195.7	−2.6	A	Pal
P14	lava flow	0/0	7/6//1	206.2	40.1	3.9	254	206.2	40.1	A	Pal
P15[c]	ignimbrite	0/0	8/8/0	39.4	−47.9	2.6	450	39.4	−47.9	A	Pal
Mean IS				28.8	−47.7	8.3	28				
Mean TC						**8.0**	**30**	**29.7**	**−49.6**		
Central Valley Domain: Locality CV4, Paleocene (West of Sierra Exploradora)											
P16[b]	sill	270/15	5/5/0	278.8	58.0	5.5	191	299.8	52.8	A	Pal
P18	lava flow	333/28	7/7/0	202.1	37.5	1.7	1383	177.9	54.9	A	Pal
P19	lava flow	10/17	11/11/0	200.4	40.1	2.9	248	185.7	40.9	A	Pal
P20	lava flow	0/0	7/7/0	39.8	−32.0	2.7	495	39.8	−32.0	A	Pal
P21	lava flow	241/16	9/9/0	1.7	−50.3	2.5	409	16.4	−62.9	A	Pal
P22	lava flow	112/18	11/11/0	9.3	−47.6	3.5	168	12.1	−30.3	A	Pal

Table 1. (continued)

Site	Lithology	S/D	N/n/p	In Situ Dec	In Situ Inc	α95	k	Tilt Corrected Dec	Tilt Corrected Inc	Type	Age
P23	stock	0/0	8/6/2	209.4	54.2	5.4	116	209.4	54.2	A	Pal
P24	lava flow	0/0	7/7/0	19.0	−49.4	3.7	263	19.0	−49.4	A	Pal
P25	lava flow	0/0	7/7/0	17.6	−54.0	3.9	236	17.6	−54.0	A	Pal
P26	lava flow	0/0	9/9/0	24.2	−48.4	6.2	69	24.2	−48.4	A	Pal
P27	lava flow	0/0	11/11/0	340.6	−69.9	3.1	216	340.6	−69.9	A	Pal
P28	lava flow	0/0	10/10/0	333.3	−60.1	3.9	151	333.3	−60.1	A	Pal
P29	lava flow	0/0	7/3/4	44.1	−39.5	7.9	68	44.1	−39.5	A	Pal
P30	lava flow	0/0	10/10/0	212.3	30.9	3.7	175	212.3	30.9	A	Pal
P31	lava flow	0/0	11/11/0	233.2	49.4	1.6	811	233.2	49.4	A	Pal
P32	lava flow	0/0	9/9/0	198.0	24.8	4.3	146	198.0	24.8	A	Pal
Mean IS				22.0	−47.4	8.5	21				
Mean TC						**9.1**	**19**	**20.5**	**−48.4**		
Precordillera Domain West of Sierra Castillo-Agua Amarga Fault: Locality P1, Jurassic (Sierra de Fraga Formation at Qdebrada Chañaral Alto)											
J06	lava flow	178/33	7/7/0	169.7	49.4	10.6	33	205.0	43.5	B/C	Pal
J07[b]	sandstones	174/60	9/2/7	137.3	42.0	7.8	53	204.5	45.6	A	J
J08	limestones	175/59	6/5/1	155.5	49.9	6.6	114	217.0	35.4	C	Pal
J10	lava flow	194/51	6/6/0	177.2	60.4	5.8	132	244.9	41.0	C	Pal
Mean IS				**165.2**	**55.1**	**14.8**	**70**				
Mean TC						23.2	29	224.0	42.4		
Precordillera Domain West of Sierra Castillo-Agua Amarga Fault: Locality P2, Jurassic (Sierra de Fraga Formation) and Late Cretaceous Intrusives (South of Cerro El Pingo)											
C12	sandstones	1/40	12/12/0	244.1	50.2	3.1	192	168.9	72.9	B	LC
C13	dike	0/0	6/6/0	349.8	−66.0	6.8	97	349.8	−66.0	A	LC
C14	dike	0/0	6/5/1	351.3	−55.2	7.3	91	351.3	−55.2	A	LC
C15	sill	21/42	8/7/1	238.1	54.1	2.3	623	171.0	56.8	A	LC
Mean IS				30.5	−61.4	26.3	13				
Mean TC						**9.5**	**95**	**350.5**	**−62.8**		
Precordillera Domain West of Sierra Castillo-Agua Amarga Fault: Locality P3, Early Eocene (Near San Pedro de Cachiyuyo)											
P33	ignimbrite	182/68	6/6/0	111.7	37.0	2.6	678	228.2	67.6	A	EE
P34	lava flow	190/52	6/6/0	161.1	47.6	8.2	67	223.7	45.4	A	EE
P35	ignimbrite	186/41	6/60	145.7	35.1	2.1	980	183.4	51.5	A	EE
P36	ignimbrite	0/0	8/8/0	229.5	75.4	1.7	1081	229.5	75.4	A	EE
P37	lava flow	271/16	8/8/0	192.7	66.4	3.7	224	211.8	81.1	A	EE
P38	lava flow	114/7	7/2/5	203.0	49.4	4.4	251	203.1	42.9	A	EE
P40	monzodiorite	193/59	8/8/0	3.1	318	192.7	58.9			A	EE
Mean IS				166.7	58.2	20.6	9				
Mean TC						**13.1**	**22**	**207.4**	**61.4**		
Precordillera Domain West of Sierra Castillo-Agua Amarga Fault: Isolated Sites (Jurassic-Late Cretaceous)											
J11	lava flow	0/0	11/10/1	26.9	−57.0	9.0	27	26.9	−57.0	A	LJ
C16	ignimbrite	51/25	6/6/0	198.6	24.6	5.6	158	192.2	9.9	A	LC
C17	lava flow	326/15	7/7/0	354.4	−53.5	7.3	68	333.2	−58.0	A	LC
C18	lava flow	326/15	8/7/1	24.8	−27.9	3.7	236	19.0	−40.3	A	LC
C19	ignimbrite	235/38	7/7/0	3.5	−57.6	7.0	74	84.6	−67.5	A	LC
C20	lava flow	239/21	7/7/0	206.7	41.7	6.7	82	226.6	50.0	A	LC
Precordillera Domain East of Sierra Castillo-Agua Amarga Fault: Locality P6, Jurassic-Eocene (Qdebrada Valiente)											
J14	limestones	251/6	7/7/0	359.7	−58.7	2.9	433	3.6	−64.4	C	LEo
J15	lava flow	156/29	9/8/1	352.5	−52.5	4.0	169	18.4	−37.9	C	LEo
C23	sandstones	175/22	9/9/0	353.1	−59.2	3.2	263	26.2	−53.5	C	LEo
C24	sandstones	175/24	10/10/0	343.6	−56.9	3.9	153	19.1	−54.3	B/C	LEo
E01	sill	265/11	5/5/0	358.7	−62.5	4.2	327	1.0	−73.7	A	LEo
Mean IS				**353.3**	**−58.1**	**4.7**	**264**				
Mean TC						13.7	32	16.1	−57.1		
Precordillera Domain East of Sierra Castillo-Agua Amarga Fault: Locality P7, Late Cretaceous-Early Eocene (Qdebrada San Andres)											
C22[b]	siltstones	45/27	4/4/0	65.7	−67.1	11.6	63	5.2	−62.0	B	EC
P45	lava flow	209/40	7/7/0	297.3	−42.7	1.5	1716	289.4	−82.1	A	PE
P46	lava flow	173/19	8/0/8	9.5	−53.1	7.1	84	28.9	−44.9	A	PE
P47	lava flow	201/23	8/8/0	322.4	−58.1	2.7	429	3.0	−73.0	A	PE
P48	lava flow	191/25	6/6/0	293.5	−57.9	8.2	67	326.2	−80.8	A	PE
P49	lava flow	162/39	6/6/0	298.4	−63.9	3.4	392	27.4	−62.8	A	PE
P50	lava flow	204/47	6/6/0	330.0	−39.8	4.4	230	29.8	−63.1	A	PE
Mean IS			6	318.8	−55.5	16.4	18				

Table 1. (continued)

Site	Lithology	S/D	N/n/p	In Situ Dec	In Situ Inc	α95	k	Tilt Corrected Dec	Tilt Corrected Inc	Type	Age
Mean TC						14.7	22	16.9	−70.0		
Mean + RTCVs			15	351.3	−57.1	11.1	13				
Mean + RTCVs			**15**			**11.4**	**12**	**40.5**	**−52.9**		
Precordillera Domain East of Sierra Castillo-Agua Amarga Fault: Isolated Sites, Jurassic-Cretaceous (Potrerillos Fold and Thrust Belt)											
J12	limestones	200/43	12/12/0	335.0	−38.6	2.7	255	**22.2**	**−56.3**	B	Ju
C21	siltstones	33/62	15/15/0	70.5	−29.8	3.7	110	**17.8**	**−44.5**	B	E
Precordillera Domain East of Sierra Castillo-Agua Amarga Fault: Isolated Sites, Late Jurassic-Early Cretaceous											
J13	limestones	145/39	5/5/0	**198.4**	**52.8**	2.3	1089	212.6	18.4	C	Eo
Precordillera Domain East of Sierra Castillo-Agua Amarga Fault: Isolated Sites, Quebrada Chañaral Alto Paleocene Early Eocene Volcanics											
P41	lava flow	179/15	7/7/0	22.0	−48.6	3.0	404	35.0	−41.1	A	PE
P42	ignimbrite	77/25	4/4/0	6.2	−57.2	3.4	750	359.4	−33.0	A	PE
P43	lava flow	172/18	6/6/0	0.8	−35.4	4.4	236	12.0	−30.9	A	PE
P44	lava flow	177/26	6/5/1	10.7	−50.1	2.0	1184	33.9	−38.6	A	PE
O01	stock	0/0	7/7/0	0.3	−85.5	6.2	96	0.3	−85.5	A	OL
Pre-Andean Depression Domain: Locality PD1, Cretaceous (Qdebrada Monardes Formation)											
C25	siltstones	193/64	10/1/9	135.1	3.4	7.1	58	161.9	51.9	A	EC
C26	siltstones	191/57	15/15/0	337.4	−10.8	6.3	37	1.2	−34.0	A	EC
Mean IS			25/16/9	333.5	−11.2	5.3	30				
Mean TC						**5.5**	**28**	**0.8**	**−38.9**		
Pre-Andean Depression Domain: Locality PD2, Cretaceous (Qdebrada Monardes Formation)											
C27	sandstones	94/17	7/7/0	157.3	71.0	2.6	536	169.2	55.5	B	Eo
C28	sandstones	62/24	5/5/0	175.5	58.0	3.0	666	167.1	34.9	C	Pal
C29	sill	0/0	10/10/0	12.1	−55.5	2.2	504	12.1	−55.5	A	Pal
Mean IS				**358.0**	**−62.1**	**17.5**	**51**				
Mean TC						10.3	144	359.0	−56.7		
Frontal Cordillera South of 27°30′S Domain:Locality FC1, Jurassic Red Beds (Rio Turbio)											
J16	siltstones	181/10	8/7/0	31.1	−42.5	3.8	258	38.0	−36.9	B/C	LEo
J17	siltstones	0/0	6/6/0	15.8	−49.8	3.1	477	15.8	−49.8	B/C	LEo
J18	siltstones	121/10	14/12/0	12.0	−47.3	5.7	60	14.7	−37.7	B/C	LEo
J19	siltstones	181/20	8/5/0	19.1	−48.3	8.1	89	36.4	−39.1	B/C	LEo
Mean IS				**19.8**	**−47.2**	**7.5**	**152**				
Mean TC						12.9	52	26.7	−41.4		
Frontal Cordillera South of 27°30′S Domain:Locality FC2, Jurassic-Cretaceous (Rio Figueroa- Qdebrada Paredones)											
J22	siltstones	211/50	9/9/0	5.8	−50.1	2.6	385	66.1	−44.4	B/C	LEo
J23	siltstones	339/31	9/9/0	35.3	−43.2	2.6	405	1.6	−64.3	B/C	LEo
J24	siltstones	0/0	6/6/0	17.9	−56.1	5.0	182	17.9	−56.1	B/C	LEo
J25	siltstones	191/30	9/9/0	201.0	59.6	5.1	103	236.4	44.6	C	LEo
J26	siltstones	181/30	8/8/0	6.1	−43.4	8.1	47	29.8	−34.0	B/C	LEo
C42	siltstones	300/20	6/6/0	8.9	−43.0	6.9	96	357.0	−60.9	B/C	LEo
C44	siltstones	191/25	5/1/4	202.4	56.7	6.7	201	230.8	45.3	C	LEo
Mean IS				16.5	−50.8	7.6	64				
Mean TC						14.9	17	35.6	−52.4		
Stepwise	**25**%					**6.2**	**95**	**21.3**	**−52.0**		
Frontal Cordillera South of 27°30′S Domain:Locality FC3, Eocene (Río Cachitos)											
E02	siltstones	255/33	11/10/0	190.0	24.7	2.9	276	204.7	53.0	B	LEo
E05	siltstones	221/10	7/5/2	232.9	61.4	11.0	32	249.1	57.9	B	LEo
E06	siltstones	301/20	10/10/0	220.5	44.2	3.2	222	226.2	63.5	B	LEo
E07	siltstones	307/48	6/6/0	220.7	13.0	3.5	368	224.5	61.0	B	LEo
E08	siltstones	325/23	5/5/0	236.0	31.3	7.2	113	236.5	54.3	B	LEo
E09	stock	0/0	5/5/0	80.2	−66.4	4.6	273	80.2	−66.4	A	LEo
E10	stock	0/0	6/6/0	197.0	56.3	3.5	365	197.0	56.3	A	LEo
Mean IS				219.3	−44.4	19.8	10.2				
Mean TC						**9.3**	**43**	**226.7**	**60.6**		
Frontal Cordillera South of 27°30′S Domain:Oligocene (Río Nevado)											
O08	siltstones	11/10	9/6/0	203.0	53.2	**8.4**	**65**	**189.4**	**54.2**	A	Ol-M

Table 1. (continued)

Site	Lithology	S/D	N/n/p	In Situ Dec	In Situ Inc	α95	k	Tilt Corrected Dec	Tilt Corrected Inc	Type	Age
Frontal Cordillera South of 27°30′S Domain:Isolated Sites											
J27	limestone	11/54	8/5/0	58.4	−48.8	4.4	305	334.9	−56.6	C	Pal
C34	ignimbrite	11/45	7/6/1	197.8	60.8	8.9	49	140.9	41.2	C	Eo-Ol
P52	ignimbrite	181/40	5/5/0	344.7	−56.0	3.5	472	38.5	−47.4	A	Pal
C30	sill	161/20	5/5/0	17.1	−58.9	11.5	45	35.1	−44.4	A	Cr
C31	sill	0/0	5/5/0	30.2	−33.2	4.5	294	30.2	−33.2	A	Cr
C32	lava flow	191/30	8/6/0	14.3	−78.9	3.4	418	79.6	−57.5	A	Cr
C33	lava flow	191/30	6/6/0	15.7	−38.5	10.6	40	36.0	−30.3	A	Cr
Neogene Ignimbrites: Cerro La Ola and Rio Juncalito Ignimbrites (23 Ma)											
O03	ignimbrite	181/10	12/12/0	117.0	60.2	1.7	627	128.1	68.7	A	
O04	ignimbrite	0/0	11/11/0	129.0	67.5	2.2	448	129.0	67.5	A	
Mean IS				122.2	64.0						
Mean TC								**128.6**	**68.1**		
Neogene Ignimbrites: Rio Frio Ignimbrite (18 Ma)											
O02	ignimbrite	0/0	8/8/0	353.4	−40.2	2.4	555	353.4	−40.2	A	
M03	ignimbrite	251/6	10/10/0	351.6	−30.7	3.0	264	352.4	−36.6	A	
M04	ignimbrite	0/0	10/10/0	353.7	−36.4	2.9	302	353.7	−36.4	A	
M05	ignimbrite	0/0	7/7/0	353.6	−41.5	2.8	477	353.6	−41.5	A	
Mean IS				353.0	−37.2	5.6	272				
Mean TC						**3.0**	**959**	**353.3**	**−38.7**		
Neogene Ignimbrites: Cuesta del Jardín, Ines Chica and Los Cristales Ignimbrites (17–15 Ma)											
M02	ignimbrite	150/4	10/10/0	320.4	−60.4	3.7	170	327.5	−60.8	A	
M06	ignimbrite	0/0	9/9/0	333.1	−60.3	3.2	257	333.1	−60.3	A	
M07	ignimbrite	0/0	9/9/0	332.9	−61.0	2.2	560	332.9	−61.0	A	
Mean IS				328.8	−60.7	5.5	508				
Mean TC						**2.4**	**2582**	**331.2**	**−60.7**		
Neogene Ignimbrites: Maricunga Ignimbrite (14 Ma)											
M08	ignimbrite	0/0	6/6/0	204.5	52.0	2.0	1139	204.5	52.0	A	
Mean Neogene ignimbrites		4			**21.3**	**20**	**165.4**	**57.3**			

[a]S/D, bedding attitude parameters; N/n/p, number of demagnetized samples/number of lines/number of planes used in the calculation of the mean direction; Dec, Inc, mean declination and inclination in situ and after tilt correction; α95, semiangle of 95% of confidence; k, Fisher's precision parameter; type of magnetization, age of magnetization. Bold indicates the site-mean characteristic directions used to calculate tectonic rotations.
[b]Rejected from the mean calculation.
[c]Special features are recognized; see text for explaination.

sition of isothermal remanent magnetization (IRM) and the variation of susceptibility during heating (K-T) on characteristic samples. IRMs were given with an ASC pulse electromagnet and K-T experiments were done with the AGICO KLY3-CS3 instrument. For most cores, one specimen was subjected to stepwise thermal demagnetization (10 to 15 steps) in an ASC furnace where the residual field was less than 10 nT. Magnetic susceptibility was measured after each thermal demagnetization step, in order to check magnetic mineralogical changes upon heating. Stepwise alternating field (AF) demagnetization using the Molspin AF instrument was also performed on some samples. Magnetization directions were determined with 'least squares lines and planes' programs according to *Kirschvink* [1980]. Evidence for secondary overprint due to lightning was found at a few sites in volcanic rocks. In these cases, AF demagnetization was preferred to thermal. Statistics combining directions and planes [*McFadden and McElhinny*, 1988] were used to determine the mean characteristic directions for such sites.

3.3. Reference Poles

[13] *Lamb and Randall* [2001] developed a technique allowing paleomagnetic poles to be calculated from a mixture of declination and inclination data drawn from localities in stable South America and the Andes. *Lamb and Randall* [2001] also attempted to correct for compaction in sedimentary rocks. The apparent polar wander path (APWP) obtained following this interesting approach is not significantly different from the one given by *Roperch and Carlier* [1992] but shows significant discrepancies with the APWP used by *Randall* [1998]. *Besse and Courtillot* [2002] have updated several APWPs for most continents. Their new SA APWP (hereafter labeled BC02) is in good agreement with the *Lamb and Randall* [2001] APWP. The BC02 APWP is the most detailed and reliable APWP and it should henceforth be used to calculate tectonic rotations.

4. Magnetic Properties

[14] During thermal demagnetization, a group of samples showed univectorial magnetizations going through the ori-

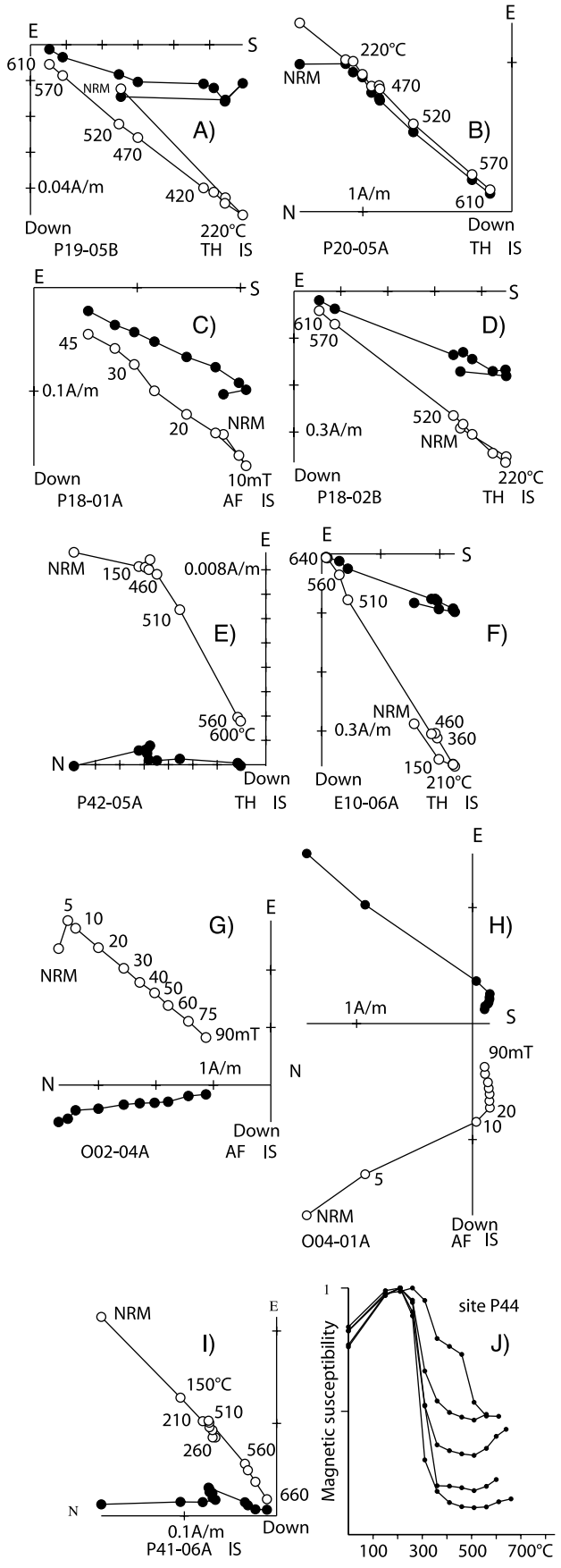

gin. Almost all samples collected from sites in volcanic and intrusive rocks fall within this category (noted type A in Table 1) except a few sites in Jurassic volcanics. In contrast, samples from most sites drilled in sedimentary rocks displayed secondary magnetization with characteristic vectors defined in the range of unblocking temperatures 150–610°C for red beds or 200–400°C for limestones. Fold tests performed at each locality (Table 1) indicate that these characteristic magnetizations were acquired either before (type B), during (type B/C) or after the sedimentary beds were tilted (type C).

4.1. Magnetization in Volcanic and Intrusive Rocks

[15] Most sites show natural remanent magnetization (NRM) intensity in the range 0.1–1 A/m and magnetic susceptibilities above 0.01SI typical of volcanic rocks with magnetite as the main ferromagnetic mineral (auxiliary material). Sites with lower magnetic susceptibility correspond to ignimbrites with a more oxidized state. The relatively low Koenigsberger ratio (remanent/induced) suggests that a certain amount of low-temperature alteration may have reduced the intensity of the NRM. Most sites in late Cretaceous to Oligo-Miocene volcanics show stable magnetization and the principal component of magnetization going through the origin during thermal or AF demagnetization (Figures 3a–3f). In most cases, the maximum unblocking temperature was higher than 580°C, the Curie point of magnetite. All fractions of the magnetization left above 580° show the same direction than the magnetization carried by magnetite indicating that oxidation during emplacement produced a small amount of hematite or stable maghemite IRM acquisitions (Figure 4a) show that although magnetite is the main magnetic carrier saturation was often incomplete at 300 mT in agreement with unblocking temperatures above 580°C. Intrusive rocks have usually magnetite as the main magnetic carrier as shown by unblocking temperatures lower than 580°C and IRM acquisition. AF demagnetization of late Oligocene–early Miocene ignimbrites show a very stable primary magnetization (Figure 3g) with, in some cases, an overprint likely related to lightning strikes which was easily removed by AF demagnetization (Figure 3h). Evidence of low-temperature oxidation was observed at some sites (P41, P44, Figures 3i and 3j) as a large decrease in magnetic susceptibility in the temperature range 250–400°C indi-

Figure 3. (a–i) Orthogonal projections (in situ) of thermal (temperatures in °C) or alternating field (steps in mT) demagnetization diagrams for samples from volcanic or intrusive rocks. The secondary overprint is removed during the first steps of demagnetization and the characteristic component is defined linearly through the origin. Solid (open) circles correspond to projection onto the horizontal (vertical) plane. (j) Variation of magnetic susceptibility (normalized) measured at room temperature during thermal demagnetization for one sample from Paleocene volcanics.

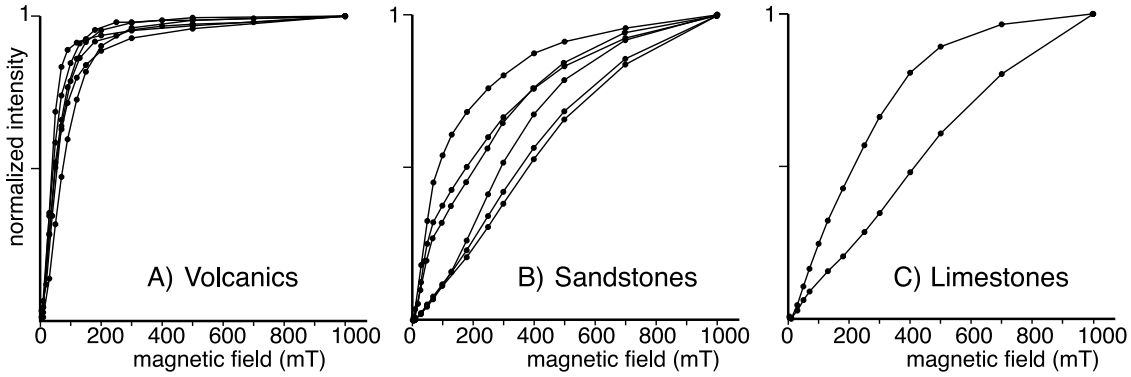

Figure 4. Normalized intensity of IRM versus magnetic field. (a) Magnetite the main magnetic carrier in extrusive and intrusive rocks. (b) Hematite the main magnetic carrier in red beds, although a small amount of magnetite is suggested by the rapid increase in IRM acquisition below 100 mT. (c) In limestones where IRMs indicate that magnetite is not the magnetic carrier. Taking into account the unblocking temperatures of NRM around 300–340°C, pyrrhotite is the most likely magnetic carrier.

cating inversion of titanomaghemite to hematite upon heating. Antipodal magnetization associated with maghemitization was also found at some sites. The ChRM above 400°C is well defined but it is unclear whether the primary magnetization was replaced by a late secondary magnetization during maghemitization.

4.2. Magnetization in Sedimentary Rocks

4.2.1. Red Beds

[16] Except at three sites (C25, C26, O08) where the ChRM is the one carried by high unblocking temperatures above 600°C (sample O0809A, Figure 5j), the characteristic magnetizations identified in the studied red beds correspond to a magnetization with unblocking temperatures almost linearly distributed in the temperature range 150–560°C up to 670°C and usually not going through the origin during thermal demagnetization (Figures 5a–5g). The ChRM was determined by least squares fit not anchored to the origin in the temperature interval 150–600°C. For example, at site C08, the ChRM of reverse polarity is well defined (sample C0813A, Figure 5c) but the high-temperature component of normal polarity observed above 600°C cannot be determined (Figure 5d). The magnetic vector is well defined and homogeneous within sites constituting a short sedimentary sequence ($\leq$10 m thick). IRM acquisition indicates that the main magnetic mineralogy corresponds to a high-coercivity magnetic mineral (Figure 4b) likely to be hematite but the rapid increase in IRM acquisition indicate that some samples have also a small amount of magnetite.

4.2.2. Limestones

[17] Most samples from sites in limestones have characteristic magnetizations with a narrow unblocking temperature range near 300°C (Figures 5k and 5l). IRM acquisition indicates the presence of a magnetic phase with magnetic saturation above 300 mT indicating that this phase is not titanomagnetite (Figure 4c). Considering that the characteristic magnetization is a secondary magnetization (Figure 5), pyrrhotite is likely the main magnetic carrier.

5. Characteristic Directions

[18] As observed during thermal demagnetization, in most sediments studied the ChRM is a secondary magnetization in most sediments studied. Magnetization is of both polarities and a single short remagnetization event is therefore discarded. As our sampling area corresponds to the location of active volcanic arcs during the Mesozoic and Tertiary, it is not surprising that remagnetizations are widespread. Remagnetization is especially noticeable in sediments but it was not recognized in the late Cretaceous or Paleogene volcanic units. Porous sandstones and siltstones with weak primary magnetization may have been easily remagnetized by fluid flow during the emplacement/intrusives of high-level. Remagnetization may occur before, after or even during tilting of sedimentary beds. For each locality, the fold test is used to assess the origin of the ChRM.

[19] One of the major difficulties for any paleomagnetic study is to attribute an age to the magnetization. Here remagnetization is thought likely to be associated with heating or fluid flow related to Paleocene and Eocene arc development. The age of the remagnetization was therefore considered to be the age of the most recent intrusive events within the sampling area.

[20] In order to discuss the tectonic implications of the paleomagnetic results and detect possible spatial variations in the amount of rotation, sites belonging to a homogeneous tectonic block were grouped into ''localities'' according to the nature and age of the magnetization. Tectonic rotations and inclination anomalies were calculated for Mesozoic-Cenozoic units, using the estimated age of magnetization and the BC02 APWP. The site-mean directions for each locality and the tectonic rotations and inclination errors are given in Table 2.

5.1. Coastal Cordillera (*CC*)

[21] Two localities were sampled within the Coastal Cordillera (Table 1 and 2 and Figures 1 and 2a–2c).

5.1.1. Locality CC1, Chañaral

[22] Normal and reverse polarity magnetizations were found in NE oriented Jurassic dikes (sites J01 and J02) while an antipodal magnetization was also found at site J02.

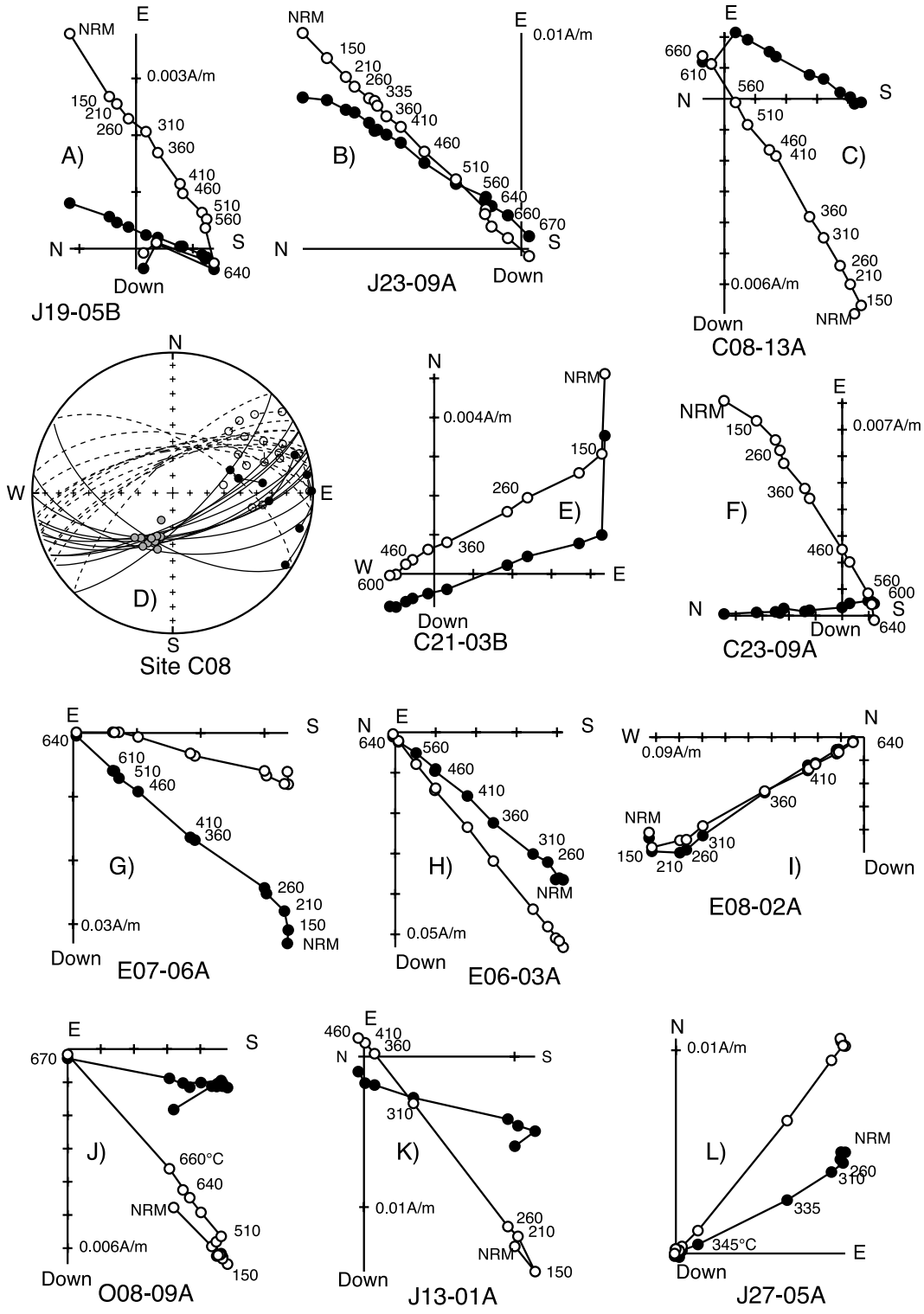

Figure 5

Table 2. Tectonic Rotations in the Atacama Region[a]

Location	Age	Latitude	Longitude	Observed			Expected		Rotation		Inclination Error	
				Dec	Inc	α95	Dec	Inc	R	±∂R	I	±∂I
RCOVe[b]	180	−26.365	−70.490	48.5	−50.4	10.0	13.0	−45.8	35.5	14.4	4.6	10.9
RCOFl[c]	150	−26.568	−70.655	50.0	−44.3	6.7	3.6	−48.4	46.4	9.5	−4.1	7.9
CC2 + CV1a	130	−25.510	−70.370	19.2	−42.1	12.3	355.3	−35.4	23.9	14.7	6.7	13.1
CV1b	80	−25.940	−69.860	30.3	−47.5	16.8	355.2	−36.0	37.6	21.1	8.4	15.5
CV2	60	−26.970	−69.990	34.3	−63.0	9.4	352.5	−49.9	41.8	17.3	13.1	8.4
CV3	60	−25.120	−69.750	29.7	−49.6	8.0	352.6	−47.9	37.1	10.7	1.7	7.6
CV4	60	−25.780	−69.500	20.5	−48.4	9.1	352.6	−48.7	27.9	11.7	−0.3	8.3
P1	60	−26.670	−69.560	345.2	−55.1	14.8	352.5	−49.7	−7.3	21.6	5.4	12.5
P2	70	−26.800	−69.610	350.5	−62.8	9.5	351.4	−45.2	−0.9	17.5	17.6	9.0
P3	55	−26.760	−69.740	27.4	−61.4	13.1	352.5	−49.7	34.9	23.0	11.7	11.2
P6	40	−26.660	−69.420	353.3	−58.1	4.7	354.1	−54.8	−0.8	10.1	3.3	6.9
P7[d]	60	−26.890	−69.490	40.6	−52.9	11.4	352.5	−49.9	48.1	15.8	3.0	9.9
PD1	130	−26.570	−68.970	0.8	−38.9	5.5	355.1	−37.1	5.7	8.4	1.8	9.5
PD2	50	−26.550	−69.290	358.0	−62.1	17.5	357.3	−53.4	0.7	32.2	8.7	14.4
FC1	40	−27.810	−69.490	19.8	−47.2	7.5	354.0	−55.9	25.8	11.5	−8.7	8.3
FC2	40	−27.630	−69.430	21.3	−52.0	6.2	354.0	−55.7	27.3	10.9	−3.7	7.5
FC3	40	−28.020	−69.450	46.7	−60.6	9.3	354.0	−56.1	52.7	17.0	4.5	9.3
M01[e]	10	−27.238	−70.963	351.6	−38.5	4.4	357.3	−50.3	−5.7	5.4	−11.8	4.5
C21[e]	130	−26.182	−69.251	17.8	−44.5	3.7	355.1	−36.5	22.7	7.4	8.0	9.0
J12[e]	160	−26.369	−69.308	22.2	−56.3	2.7	358.0	−45.2	24.2	7.5	11.1	7.4
J13[e]	35	−26.482	−69.433	18.4	−52.8	2.3	354.5	−51.0	23.9	5.4	1.8	4.5
O08[e]	25	−27.854	−69.267	9.4	−54.2	8.4	358.2	−52.7	11.2	12.6	1.5	8.1
Ritr1	200	−27.670	−69.420	33.1	−51.1	6.5	8.9	−55.4	24.2	10.0	−4.3	6.9
RiEb	60	−27.570	−70.170	46.8	−45.0	5.2	352.4	−50.6	54.4	7.1	−5.6	5.6
Riqm	130	−27.620	−69.520	23.7	−40.9	20.5	355.1	−38.5	28.6	22.9	2.4	18.3
RiCS	80	−27.650	−69.637	21.6	−48.5	22.9	352.6	−41.5	29.0	29.4	7.0	19.8
RTCVn	60	−26.482	−69.381	40.1	−38.5	12.1	352.5	−49.5	47.6	13.1	−11.0	10.4
RTCVs	60	−26.820	−69.531	47.5	−40.5	10.7	352.5	−49.8	55.0	12.0	−9.3	9.4
RTQCB	130	−26.801	−69.497	27.8	−39.5	11.6	355.1	−37.3	32.7	13.6	2.2	12.5
RTQCn	130	−26.649	−69.399	358.5	−47.8	8.3	355.1	−37.1	3.4	11.7	10.7	10.7
RTQCn	130	−26.649	−69.399	1.0	−38.3	10.6	355.1	−37.1	5.9	12.5	1.2	11.9
RTmnv	130	−26.475	−69.430	326.6	−36.2	11.6	355.1	−36.9	−28.5	13.1	−0.7	12.5
RCoLN	180	−25.990	−70.477	42.0	−35.5	9.6	12.9	−45.3	29.1	11.7	−9.8	10.8
RCOVe	180	−26.365	−70.490	48.9	−49.6	12.1	13.0	−45.8	35.9	16.6	3.8	12.2
RCOFl	150	−26.568	−70.655	45.6	−43.0	8.8	3.6	−48.4	42.0	11.3	−5.4	9.2
RCOLA	150	−26.342	−70.430	44.0	−48.6	11.2	3.6	−48.1	40.4	14.8	0.5	10.7
RCOLT	130	−26.490	−70.360	38.7	−41.5	12.0	355.2	−36.8	43.5	14.3	4.7	12.8
RCORe	120	−26.690	−70.277	37.2	−39.3	11.6	354.8	−40.0	42.4	12.3	−0.7	9.9
T2	50	−27.300	−70.200	34.1	−41.7	5.0	357.1	−54.2	37.0	6.7	−12.5	5.3
T3	60	−27.500	−70.100	25.8	−42.7	9.3	352.4	−50.5	33.4	10.9	−7.8	8.4
T5	70	−27.700	−70.200	29.3	−42.1	8.0	351.3	−46.2	38.0	9.7	−4.1	7.9
T6	50	−27.700	−70.100	42.2	−44.3	10.2	357.1	−54.6	45.1	12.2	−10.3	8.8
T7	65	−28.400	−70.500	27.9	−54.3	8.3	350.9	−47.8	37.0	11.9	6.5	7.5

[a]Latitude, longitude, position of the localities used in the calculation of the tectonic parameters; $R \pm \partial R$, $I \pm \partial I$, rotation and inclination error parameters and their associated errors [*Demarest*, 1983]; localities CC (Coastal Cordillera), CV (Central Valley), P (Precordillera), PD (Pre-Andean Depression), and FC (Frontal Cordillera) from this study; localities Ri from *Riley et al.* [1993]; localities RC from *Randall et al.* [1996]; localities RT from *Randall et al.* [2001]; localities T from *Taylor et al.* [2002]. Age is the age (in Ma) of the reference pole after *Besse and Courtillot* [2002] used to calculate the rotation.
[b]SiteJ01+RC0VE.
[c]SiteJ02+RC0FL.
[d]P7+RTCVs.
[e]Calculated rotations for single sites.

Figure 5. Orthogonal projections (in situ) of thermal demagnetization diagrams for samples from (a–j) red beds and (k and l) limestones. In most cases the characteristic magnetization corresponds to a vector not going through the origin during demagnetization. In red beds, the direction was determined in the temperature range 150–600°C. The unblocking temperatures of the characteristic magnetization in limestone are in the range 250–400°C, suggesting pyrrhotite as the main magnetic carrier. For site C08 (equal-area stereonet), the ChRM directions are shown in gray circles. The magnetization left in the samples above 600°C is scattered and great circles analysis only enable the determination of the low-temperature component (gray circles). Legend is same as in Figure 3 for orthogonal plots. Solid (open) circles correspond to projection into the lower (upper) hemisphere of the stereonets.

This low unblocking magnetization is probably carried by maghemite as suggested by a decrease in magnetic susceptibility during heating. Primary and secondary magnetizations are antipodal suggesting that both magnetizations can be considered of similar age in the calculation of tectonic rotations. The characteristic directions have NE-SW declinations in agreement with those reported by *Randall et al.* [1996]. We combined these results to the Vetado (J01) and Flamenco (J02) localities of *Randall et al.* [1996] and calculated new mean directions (RCOVe and RCOFl in Table 2).

5.1.2. Caldera

[23] One site (M01) was drilled in fine-grained red mudstones intercalated within shallow water marine late Miocene-Pliocene sediments of the Caldera Formation along the Pacific shore near Caldera (Figures 2a–2c). This single site in late Neogene sediments shows no evidence of rotation although further work is needed to confirm this preliminary result.

5.2. Central Valley (*CV*)

[24] Four localities were defined for the Central Depression (Tables 1 and 2 and Figure 2a).

5.2.1. Locality CV1a, North of Diego de Almagro

[25] Reverse polarities ChRMs were recorded at three sites drilled in late Jurassic–early Cretaceous lavas (J03–J05). This locality also includes two other sites drilled in the upper part of La Negra Formation and an early Cretaceous intrusive, farther to the west, on the eastern side of the Coastal Cordillera (Figure 1 and Table 1). A mean direction was calculated for this locality for comparison with results obtained by *Randall et al.* [1996] in Jurassic rocks which outcrop to the west of the Atacama Fault System. The good stability of the magnetization indicates that the magnetization is very likely primary but the fold test is not conclusive (Table 1 and Figure 6).

5.2.2. Locality CV1b, North of Diego de Almagro

[26] Normal and reverse magnetizations were observed in the late Cretaceous volcanics (Llanta Formation) and related intrusives (C04–C07). The reverse component at site C06[2] was included in the mean calculation although it is a secondary component, which may be related to a nearby Late Cretaceous intrusion. Bedding is near horizontal for this site, therefore using the tilt-corrected or in situ direction will not change the locality-mean result (Figure 6).

5.2.3. Locality CV2, South of Inca de Oro

[27] Secondary magnetizations were found in early Cretaceous limestones from the Chañarcillo Group (for example, site C08, Figures 5c and 5d). Although bedding is nearly horizontal at site C11, bedding attitude varies slightly within the site and dispersion decreases upon tilt correction. This suggests that the remagnetization in the limestones was acquired prior or during folding. Sites C09 and C10 are close to a major fault and a hydrothermal alteration zone and were likely remagnetized while the fault was active. A primary magnetization was determined in a monzodiorite stock (site P39) after removal of overprints due to lightning. We assume that the remagnetization in sediments occurred during late Cretaceous–early Paleocene, the age of most intrusives in the area. Site P39 primary ChRM (Table 1) was averaged with the secondary components determined in sediments. The best grouping of the paleomagnetic directions occurred with stepwise unfolding at 25% (Figure 7).

5.2.4. Locality CV3, Catalina-Aguas Blancas

[28] Fifteen sites (P01 to P15) on Paleocene volcanics from the northern part of the studied area (Figures 2a–2c). Two sites (P15 and P06), one kilometer apart, correspond to the same ignimbrite as shown by field evidence and identical magnetic properties. A mean direction based on the data from both sites was taken in order not to overweight a particular unit prior to calculating the locality-mean direction. Two sites with directions at more than 40° from the mean direction were also removed (Table 1). Because bedding is mostly horizontal, the fold test was inconclusive (Figure 6).

5.2.5. Locality CV4, Sierra Exploradora

[29] Seventeen sites in Paleocene volcanics and intrusives (P16–P32, Table 1 and Figures 2a–2c). Site P16, corresponds to Paleocene volcanoclastic sandstones and related sill. The magnetization in the sandstones was unstable and an intermediate direction, at more than 40° from the mean, was observed in the sill and this direction was removed from the mean calculation. The units are almost flat lying and a tilt correction was only applied at 4 sites. The mean direction for the 15 units is, as for locality CV3, the same before and after applying the tilt correction (Figure 6).

5.3. Precordillera (*P*)

[30] Extensive sampling was carried out in the Precordillera both to the east and west of the Sierra del Castillo–Agua Amarga Fault (SCAMF, Figures 2a–2c).

5.3.1. Area West of the Sierra Castillo–Agua Amarga Fault

5.3.1.1. Locality P1, Quebrada Chañaral Alto

[31] The oldest sites west of the SCAMF correspond to lava flows and sediments of the middle to late Jurassic Sierra de Fraga Formation (Table 1). Both the volcanics (J06, J10) and limestones (J08, Figure 6) show secondary magnetizations and reverse polarities. The remagnetization may have been acquired during the late Cretaceous to early Eocene interval as a consequence of the emplacement of shallow level intrusives, which outcrop nearby. Red volcanoclastic sediments at site J07 (not considered for the mean calculation) record a secondary overprint in the present-day field and a reverse polarity magnetization at high temperatures, which may correspond to a pretectonic remanent magnetization.

5.3.1.2. Locality P2, South of Cerro El Pingo

[32] In this locality a secondary magnetization was found at site C12, (siltstones of the Jurassic Sierra de Fraga Formation). The direction is similar to the primary magnetization found in a sill (C15) intruding the sedimentary sequence. As the sill parallels to bedding, a bedding correction was applied to the characteristic directions recorded in both the sill and sediments. Tilt corrected directions are antipodal to the normal polarity directions recorded by late Cretaceous intrusives at sites C13 and C14.

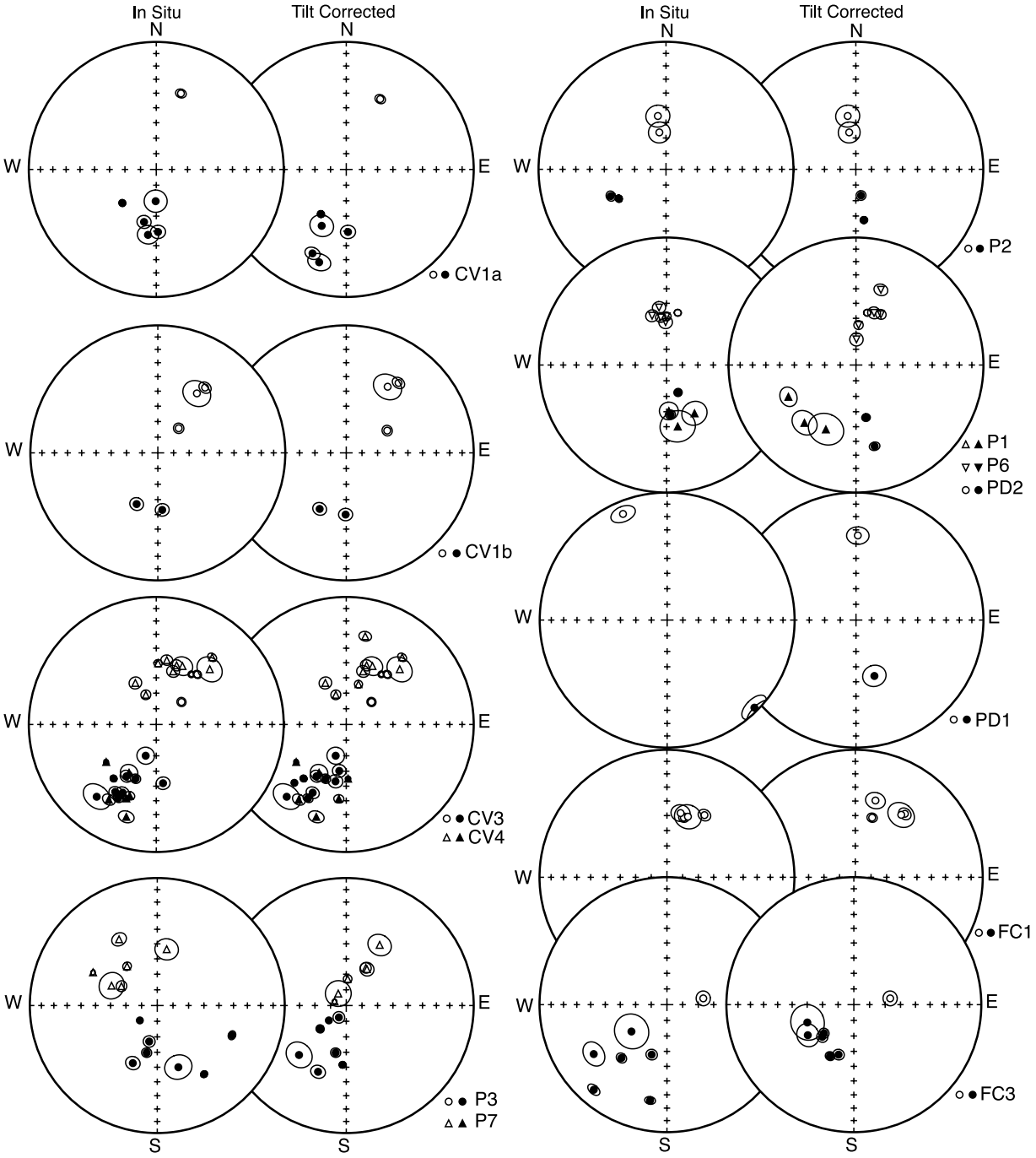

Figure 6. Equal-area projection of site-mean characteristic directions (left) in in situ (IS) and (right) after tilt correction (TC) for localities listed in Table 2. Open (solid) symbols correspond to projection in the upper (lower) hemisphere.

Dike C13 is vertical and there is no evidence for a tilt correction to be applied. The locality-mean direction was calculated averaging both the tilt corrected (C12, C15) and in situ directions from the two intrusives (C13, C14, Figure 6).

5.3.1.3. Locality P3, San Pedro de Cachiyuyo

[33] Sites P33–P38 were drilled in early Eocene volcanics (55–51 Ma [*Matthews et al.*, 2006]) while a Paleocene-Eocene intrusive was sampled in the same area at Quebrada Chañaral Alto (P40). Magnetization of reverse polarity, with high unblocking temperatures, is well defined in all sites. The fold test gave positive results (Table 1 and Figure 6).

5.3.1.4. Isolated Sites

[34] These sites were drilled in late Cretaceous (85–64 Ma) Llanta Formation volcanics at Quebrada San Andrés–

Paipote (C17, C18, C19), along the road from Diego de Almagro to El Salvador (C20) and on the road from El Salvador to Potrerillos (C16) (Figure 2b). Results are presented in Table 1.

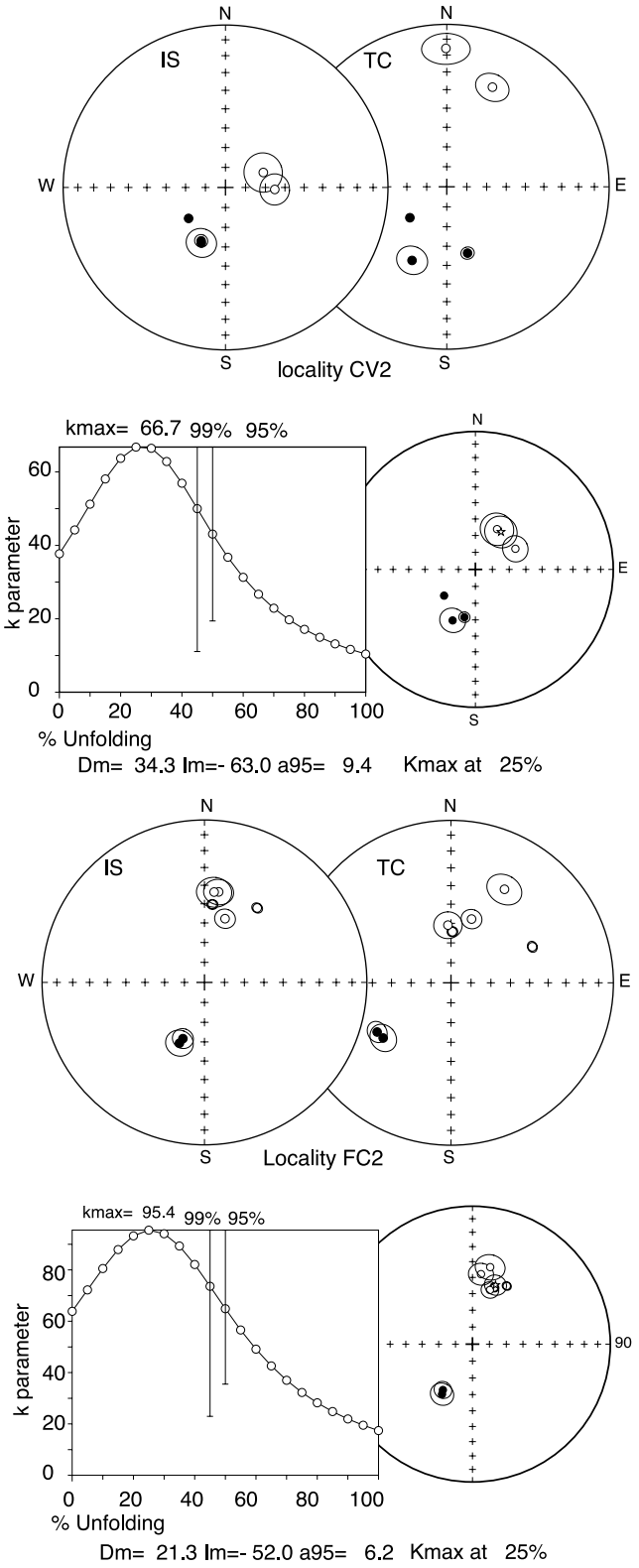

Figure 7. Equal-area projection of site-mean characteristic directions (left) in in situ and (right) after tilt correction for localities CV2 and FC2. The Fisher parameter *k* increases with partial unfolding, suggesting the existence of a syntectonic magnetization (graphs made with PaleoMac software [*Cogné*, 2003]).

5.3.2. Area East of the Sierra Castillo–Agua Amarga Fault

5.3.2.1. Locality P6, Quebrada Valiente

[35] Five sites were collected along the NW trending fault corridor, which extends from Potrerillos to La Coipa (Figures 2a–2c). The directions in in situ coordinates are tightly grouped for the 5 sites. Secondary magnetizations were found in limestones of the early Jurassic Montandón Formation (J14), sediments intercalated with lavas of late Jurassic–early Cretaceous Quebrada Vicuñita Formation (J15) and red sandstones from the early Cretaceous Quebrada Monardes Formation (C23, C24). At site C23, the ChRMs was determined in the temperature range 150–600°C (sample C2309A, Figure 5f). Upon demagnetization, the residual magnetic vector pass the origin and a poorly resolved magnetization of reverse polarity was observed above 640–670°C being impossible to determine the high unblocking temperature component of magnetization. Field relations at site C24 indicate local remagnetization related to a dike intrusion. As magnetization recorded by the sediments is also very similar to the magnetization found in a sill of likely Eocene age at site E01, we interpret the locality-mean direction as a posttectonic magnetization of mid to late Eocene age (Figure 6).

5.3.2.2. Locality P7, Quebrada San Andrés

[36] Seven sites were sampled in the same locality where *Randall et al.* [2001] reported large clockwise rotations. All sites show normal polarity (Table 1). After tilt correction the scatter didn't significantly decrease because strata at most sites show very similar strike and dip. The steep inclination suggests that secular variation is not well averaged. The six directions reported in Table 1 were averaged with the nine results from *Randall et al.* [2001] (Table 2, P7). Our new data for Cretaceous red sandstones of the Quebrada Monardes Formation (site C22) are in agreement with the results reported by *Randall et al.* [2001] for the same unit although rotation magnitude is a half that found in sites drilled farther west in Paleocene (Cerro Valiente Formation) volcanics.

5.3.3. Isolated Sites

5.3.3.1. Potrerillos Fold and Thrust Belt

[37] Three sites were drilled in Mesozoic sediments along the NNE trending Potrerillos Fold and Thrust Belt (PFTB, Figures 2a–2c). Samples include black shales of the Pliensbachian Montandón Formation (Quebrada Asientos, J12), marine sediments intercalated with lavas of the Oxfordian Quebrada Vicuñita Formation (J13, near mina Vieja de Potrerillos) and red siltstones of the late Cretaceous Leoncito Formation (C21) near the northwest corner of the Salar de Pedernales. At site C21, the ChRM is a normal polarity, secondary component that did not go through the origin

during demagnetization (sample C2103B, Figure 5e). As the in situ direction is far away from the expected direction and has a low inclination in contrast with the tilt-corrected direction we interpret the ChRM as a pretilt magnetization. The ChRM in the black shales (J12) is carried by magnetite and we interpret the magnetization to be a primary mid-Jurassic ChRM. At Site J13, close to the old Potrerillos copper mine, the ChRM (sample J1301A, Figure 5k) is carried by pyrrhotite. We interpret this ChRM to be a remagnetization associated with hydrothermal alteration related to porphyry copper emplacement. *Marsh et al.* [1997] indicate that cooling of the Potrerillos copper porphyry from hornblende Ar closure (550°C, 35.83 ± 0.21Ma) to biotite closure (250°C, 35.65 ± 0.04 Ma) was accomplished in less than 300 ka. Although we attribute an age of 35Ma to the magnetization at site J13, we note however that the magnetic polarity is reverse while the earth magnetic field was mostly of normal polarity in the time interval 35–40 Ma when most of the mineralization events occurred.

5.3.3.2. Quebrada Chañaral Alto

[38] Despite some maghemitization, the characteristic magnetization corresponds to a principal component of magnetization going through the origin during thermal demagnetization (sites P41–P44). We interpret the magnetization as a primary magnetization of Paleocene–early Eocene age. The low number of sites and uncertainties in bedding correction may explain the increase in dispersion upon tilt correction and the low inclination. Site O01, south of Potrerillos, is a posttectonic stock emplaced along an Incaic reverse fault during the Oligocene [*Cornejo et al.*, 1993].

5.4. Pre-Andean Depression (PD)

5.4.1. Locality PD1, Sierra Leoncito

[39] This locality groups two sites drilled in early Cretaceous red beds of the Quebrada Monardes Formation southeast of the Salar de Pedernales (Figures 2a–2c). ChRM were determined from high-temperature magnetizations with normal and reverse magnetizations observed at both sites (C26 and C25), which suggest a depositional origin for the magnetization. At site C25, the existence of a secondary magnetization due to lightning lead us to use great circles intersection to determine the site-mean characteristic direction. Although we sampled only two sites for this locality, as several beds were drilled at both sites the locality-mean direction was determined at the sample level.

5.4.2. Locality PD2, Quebrada Potrero Grande

[40] Paleomagnetic results were obtained at two sites from the early Cretaceous Quebrada Monardes Formation (sites C27, C28) and at one site from a late Cretaceous–Paleogene sill (C29, Figures 2a–2c). Magnetization at site C29 is a well-defined primary magnetization. At site C27 the characteristic magnetization was recovered from samples drilled in baked early Cretaceous sediments one meter away from an altered dike contact. A secondary magnetization of reverse polarity was found in Cretaceous red sandstones at site C28. This secondary magnetization is likely associated to Late Cretaceous–Paleogene volcanism. The in situ mean direction (Figure 6) is considered for this locality and we assume that the age of the magnetization corresponds to the age of the intrusions within the area (Late Cretaceous–Paleogene). There are only three sites for this locality but a significant amount of secular variation must have been averaged at site C28 during the remagnetization process.

5.5. Frontal Cordillera south of 27°30′S (*FC*)

[41] The northernmost part of this region (upper Copiapó river valley), was previously sampled by *Riley et al.* [1993]. They reported clockwise rotations, primary magnetization in Triassic volcanics (La Ternera Formation) and secondary magnetization in Jurassic–early Cretaceous red beds.

5.5.1. Locality FC1, Rio Turbio

[42] Secondary magnetization of normal polarity was found at all the four sites in this locality (sample J1905B, Jurassic red beds, Figure 5a). Dispersion increased upon tilt correction (Table 1 and Figure 6) indicating that magnetization was acquired after deformation. We attribute a late Eocene age to the magnetization assuming that the age of main deformation in the area is possibly middle to late Eocene.

5.5.2. Localities FC2, Rio Figueroa–Quebrada Paredones

[43] Characteristic directions in Jurassic-Cretaceous red beds are better grouped in in situ coordinates than after tilt correction (Table 1). Stepwise unfolding provides better grouping after 25% unfolding (Figure 7). We attribute a late Eocene age to these characteristic magnetizations, which are likely associated with the many late Eocene–early Oligocene plutons, stocks and dikes which in that region intrude the Jurassic strata.

5.5.3. Locality FC3, Rio Cachitos

[44] Paleomagnetic results were obtained for five sites drilled in Eocene (early Oligocene) continental sediments. Although in many samples the magnetization is a well-defined component going through the origin during demagnetization (samples E0603A, E0802A, Figure 5), the high intensities of the remanent magnetization (up to 0.1 A/m) recorded at site E06, E07 and E08 suggest that the magnetization is not detrital but likely of thermochemical origin. Dispersion decreases during tilt correction indicating that magnetization was acquired prior to the gentle deformation that affects the Eocene sequence at Río Cachitos. A small pluton, drilled at site E09, exhibit a normal polarity magnetization with a NE-E declination while the pluton drilled at site E10 records a reverse magnetization. The ChRMs of these two late Eocene stocks were mixed with those from the Eocene sediments. Upon tilt correction, dispersion decreases significantly especially for the inclination with an increase in K from 8 to 138 in Fisher statistics. Scatter in declination suggests a component of local tectonic rotation within the area.

5.5.4. Isolated Sites

5.5.4.1. Oligocene Red Siltstones, at Rio Nevado

[45] Paleomagnetic results were obtained at only one site (O08) because of the poor exposure of an evaporite-rich continental sequence of essentially Oligocene age

[*Mpodozis et al.*, in prep]. These preliminary results cannot rule out a low component of clockwise rotation (10°) during or after the Oligocene. This result, however, seems to point out that the large rotations found farther west may well be essentially older than the Oligocene.

5.5.4.2. Quebrada Carrizalillo and Quebrada Paredones

[46] Jurassic limestones from site J27 in the upper valley of Quebrada Carrizalillo (sample J2705A) show a secondary magnetization probably associated to the intrusion of the large Cuesta del Gato, Eocene, pluton (Figures 2a–2c). Magnetization acquired after the sediments were tilted, indicate a large clockwise rotation. Primary magnetization was found in a Paleocene ignimbrite sampled at site P52 and Late Cretaceous volcanics at sites C30–C34 (Figures 2a–2c). Although the results from these isolated sites are not used in the following tectonic analysis, they support the occurrence of important clockwise tectonic rotations within the studied region.

5.6. Late Oligocene–Miocene Ignimbrites

5.6.1. Cerro La Ola Dome and Río Juncalito Sequence (23–24 Ma)

[47] Site O04 corresponds to the La Ola rhyodacitic dome (K/Ar 23–24 Ma [*Cornejo et al.*, 1998]) while site O03 corresponds to an ignimbrite interbedded within the late Oligocene–early Oligocene Río Juncalito sequence [*Mpodozis and Clavero*, 2002] collected 10 kilometers to the east. Both sites record the same characteristic direction with E-SE declination and steep inclination different from the expected direction indicating that, they are probably genetically related.

5.6.2. Rio Frio Ignimbrite and Vega Helada Vitrophyre (18 Ma)

[48] A similar direction with normal polarity was found at three widely spaced sites drilled in the Río Frio Ignimbrite (circa 18 Ma [*Cornejo and Mpodozis*, 1996]) between the Salar de Punta Negra and Sierra Exploradora (M03, M04, M05, Table 1). At these sites the ignimbrite shows a characteristic vitrophyric level. Another sample (O02) was collected from a vitrophyre associated with the circa 18 Ma Vega Helada Ignimbrite [*Tomlinson et al.*, 1999] near La Ola (Salar de Pedernales). Paleomagnetic sampling confirms field observations and radiometric data indicating that rocks in all these localities belong to a very large ash flow tuff emplaced during a major volcanic collapse event of the Aguilar Caldera [*Mpodozis and Clavero*, 2002]. Paleomagnetic data also show that no significant deformation occurred, within the region where the ignimbrite was sampled after it was emplaced.

5.6.3. Los Cristales, Inés Chica, and Cuesta del Jardín Ignimbrites (17–15 Ma)

[49] Younger, mid-Miocene ignimbrites were drilled at site M06 near the headwaters of Rio de la Sal (Inés Chica Ignimbrite, 17–16 Ma [*Tomlinson et al.*, 1999]) and near Cerros Bravos (M07, Los Cristales ignimbrite, 16–15 Ma [*Cornejo et al.*, 1998]). At another site west of the SCAMF (M02) a 15 Ma ignimbrite [*Cornejo et al.*, 1993] interbedded in the middle Miocene Atacama Gravels, slightly tilted toward the west (<5°) was drilled along the road from Potrerillos to El Salvador at Cuesta del Jardín. These three middle Miocene ignimbrites show a similar paleomagnetic direction which is far away from the expected dipolar direction. As the probability that several distinct volcanic events recorded the same direction is very low the data suggest that the ignimbrites correspond to the same volcanic unit. There is no evidence for relative rotation within the area between sites M06 and M07 or with site M02 if we apply a tilt correction of 5°.

5.6.4. Maricunga Ignimbrite (14 Ma) South of Salar de Maricunga

[50] Site M08 corresponds to an isolated outcrop of the lower Maricunga Ignimbrite (14 Ma) collected to the south of Salar de Maricunga [*Mpodozis et al.*, 1995]. This ignimbrite presents a well-defined reverse direction.

[51] Paleomagnetic sampling in the ignimbrite sequence provided only four independent directions. Because of the difficulty to average secular variation, the mean direction (Dec = 350.0, Inc = −57.8; k = 25; α_{95} = 18.8) is not further discussed in the regional tectonic analysis section.

6. Tectonic Rotations Within the Southern Atacama Desert

[52] Tectonic parameters from previous studies [*Riley et al.*, 1993; *Randall et al.*, 1996; *Randall et al.*, 2001; *Taylor et al.*, 2002] were recalculated using the BC02 APWP in order to obtain a coherent database (Table 2). Statistically, the error in inclination is low (0.7 ± 7.3, Figure 8a). Rotations are mainly clockwise (29.0 ± 18.2), except for one locality for which *Randall et al.* [2001] reported significant counterclockwise rotations (Figures 8b, 8c, 8d, and 9). Their detailed structural study demonstrates that this counterclockwise rotation is associated with a particular kilometer-scale local structure [from *Randall et al.*, 2001, Figure 4]. The median rotation value (33.4) is slightly larger than the arithmetic mean indicating that the mean rotation is not skewed by a few large values. The magnitude of rotations is broadly similar in sites both in the Coastal Cordillera and Central Depression domains (Figure 8d). Sites in the Precordillera show a greater variability in the rotation pattern (Figures 8d and 9). From north to south, the magnitude of rotation coincides with the orientation of the main structures of the Precordillera Fault System (Figure 9). While rotations are observed in the N20°E oriented PFTB, no rotation is found, immediately to the south of the PFTB (26.5–27°S, Figures 8c and 9). Farther south in the Frontal Cordillera the magnitude of the clockwise rotations coincides with the orientation of the structures and the general orientation of the fault bounded Paleozoic basement blocks.

7. Age of Tectonic Block Rotations

[53] When considering the multiple events of extensional, compressional and oblique deformation, which shaped the Atacama region during the Mesozoic and Tertiary, it is

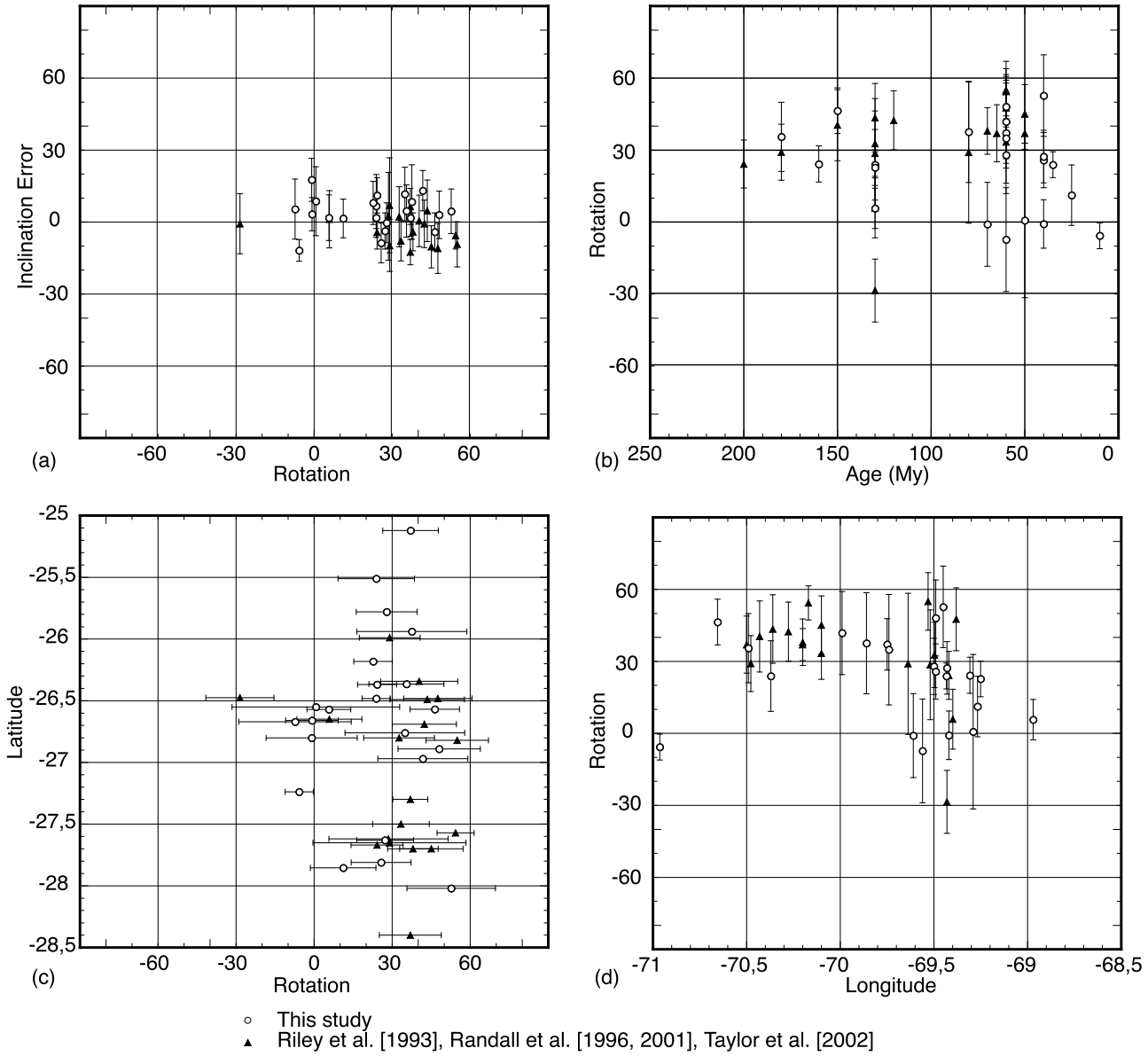

Figure 8. (a) Variation of inclination errors with rotations. (b) Variation of rotations with age of magnetization. (c) Variation of rotation with latitude (in a N-S sense). (d) Variation of rotation with longitude. Data are listed in Table 2.

tempting to assume that the tectonic rotation pattern may well be the result of the cumulative effect of superimposed deformation episodes. On the other hand, the episodic eastward migration of the Andean arcs during the Late Cretaceous and Tertiary may also have shifted eastward the locus of rotation-prone areas as a consequence of displacement of thermally weakened crust to the east following arc migration. Rotations in the Coastal Cordillera and Central Valley may be thus linked to the oldest early Late Cretaceous and early Paleocene phases of compressional/oblique deformation [*Forsythe and Chisholm*, 1994; *Randall et al.*, 1996; *Taylor et al.*, 1998] while rotations in the Precordillera can be related to the transpressional deformation associated to the Incaic tectonic phase [*Randall et al.*, 2001; *Arriagada et al.*, 2000, 2003].

[54] If this scenario is accepted, rotation magnitude should be highly variable between sites and the regional rotation pattern, geometrically very complex. However, this is not the case, as a close inspection of Table 2 and Figures 8, 9, and 10 shows that whatever the magnetization age, rotations in Jurassic and early Cretaceous units in the

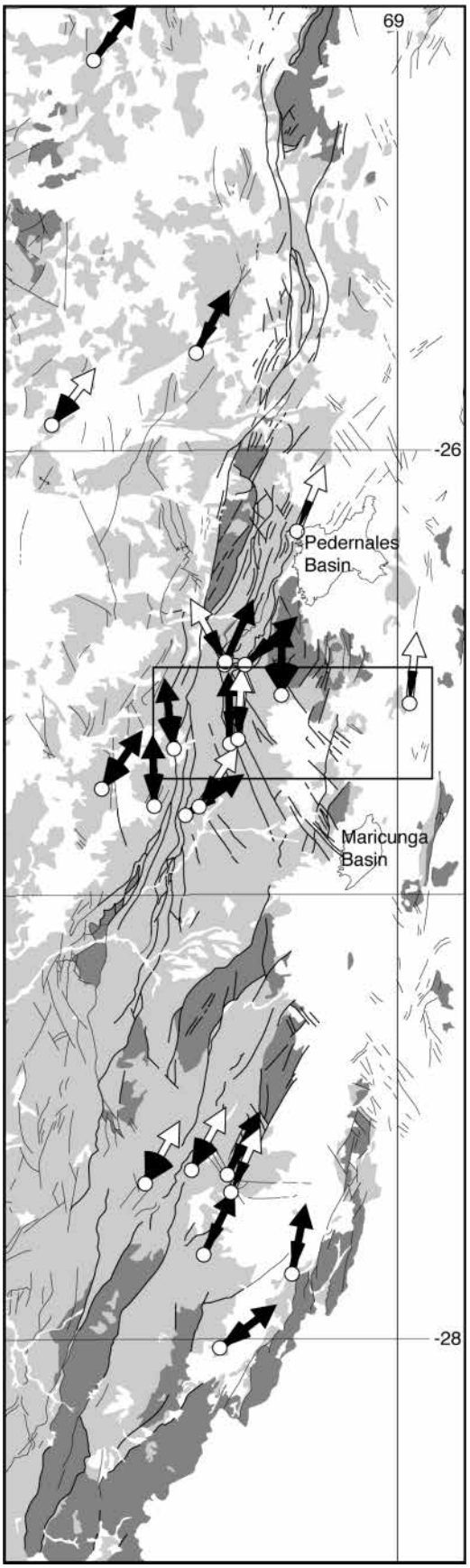

Coastal Cordillera can be compared to those found in late Cretaceous–Paleogene units in the Central Depression and Precordillera. Even though rotations in the Precordillera show variations in magnitude and sense, when the complete regional paleomagnetic data set is examined, a large-scale and coherent rotation pattern arises well beyond the potential influence of individual structural systems, specific arcs and/or tectonic domains (Figures 8, 9, and 10). The very existence of such as pattern strongly suggests that a common tectonic event is the most likely cause for most of the rotations.

[55] Paleomagnetic data from Paleocene-Eocene volcanics and intrusives, widely distributed along the Central Depression and Precordillera, showing rotations essentially with the same sense and magnitude than rotations in Mesozoic rocks indicate that no major rotation occurred before the Eocene. More precisely, data obtained from Eocene red beds from the Frontal Cordillera, south of 27°30s (locality FC3, Tables 1 and 2) constrain the maximum age of rotation to the late Eocene. The clockwise rotations recorded by remagnetizations at localities FC1 and FC2 in the Frontal Cordillera indicate a component of rotation postdating or synchronous with the estimated Eocene–early Oligocene deformation within the area. In contrast, the minimum age for the rotation is more difficult to constrain as most of the Oligocene and Neogene rocks within the Precordillera and Central Depression are unconsolidated conglomerates and gravels, not suitable for paleomagnetic studies. Our best data come from the single Site O08, at Río Nevado south of 27°30′S, in the Frontal Cordillera domain, where we sampled Oligocene fine-grained continental sediments. The magnitude of the clockwise rotation found in this site is noticeably smaller (11.2° ± 12.6°) than the rotations observed in the remagnetizations recorded at nearby localities FC1 (25.8° ± 11.5°) and FC2 (27.3° ± 10.9°), suggesting a relatively small component of rotation during the late Oligocene, after an essentially Eocene–early Oligocene tectonic event associated to important block rotations. Further work is, however, needed to confirm this preliminary result. On the other hand, the lack of evidences of internal relative rotation on Miocene ignimbrites, which overlie rotated and nonrotated rocks in the Precordillera and Pre-Andean Depression indicate that relative block rotation essentially ceased before 18 Ma, the age of Río Frío Ignimbrite that cover a large area between Salar de Punta Negra and Salar de Pedernales (Figures 2a–2c). Thus, unless the present nonrotated

Figure 9. Tectonic rotations with errors (deviations of arrows from a N-S direction) and main geological and structural features for the Precordillera and Frontal Cordillera. Dark shaded, Paleozoic basement; light shaded, Mezosoic-Paleogene rocks. The color of the arrows indicates the inferred age of the magnetization (black (20–70Ma), white (70–200)).

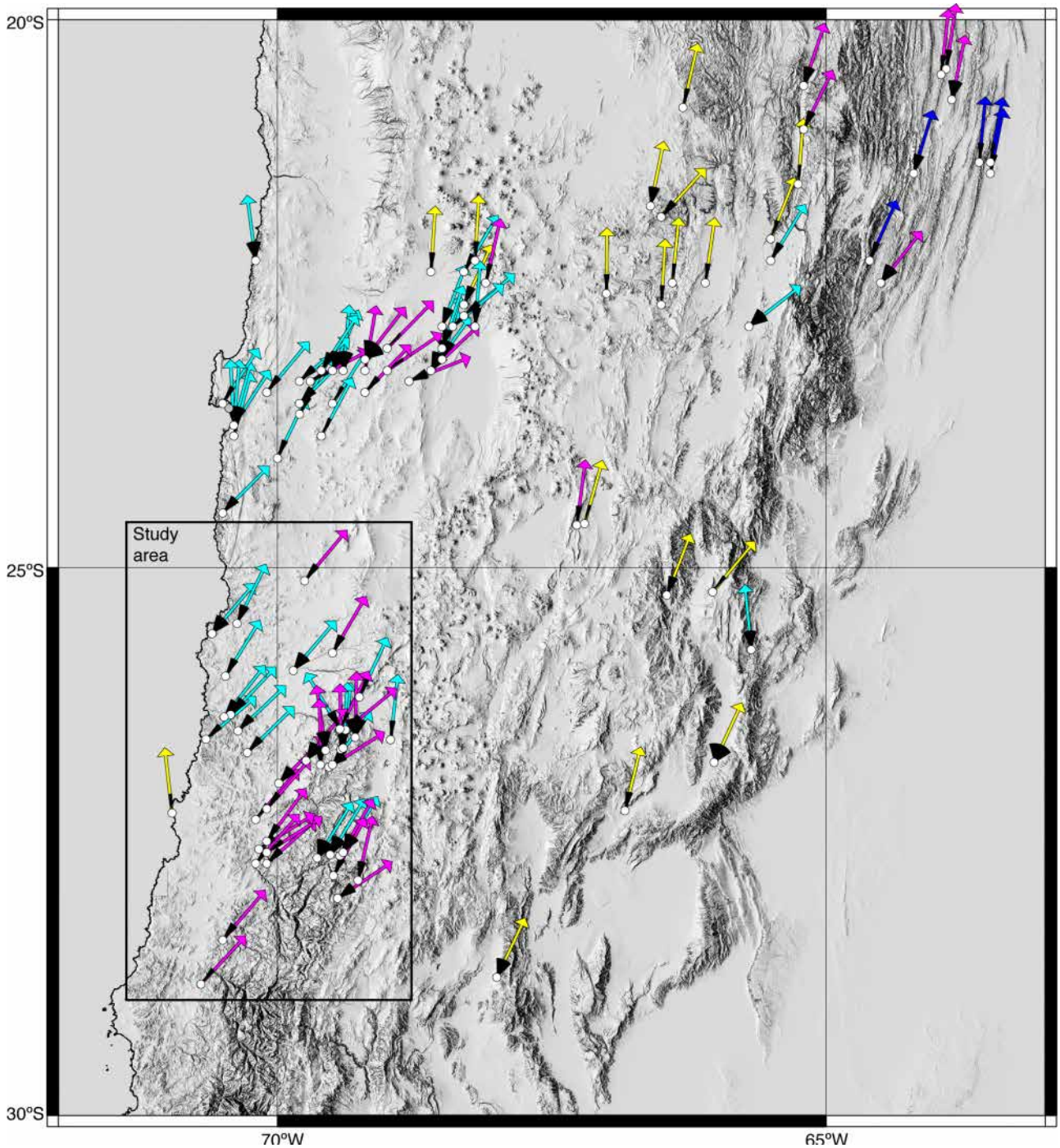

Figure 10. Compilation of tectonic rotations with errors for the central Andes between 20°S and 30°S. The rectangle shows the study area of the Atacama region. The main structural features of the Andes are well observed in the shaded topography (SRTM 90 m digital elevation model). Colored arrows show the inferred age of the magnetization. Yellow (0–20 Ma), pink (20–70 Ma), light blue (70–200 Ma), blue (200–300 Ma).

block had been rotated counterclockwise prior to be covered by the Miocene ignimbrites, our result indicates that clockwise rotations are anterior to the early Miocene. The deformation that produced the rotation in the present forearc of the southern Atacama Desert Region seems to have occurred essentially between the Eocene–early Oligocene (40–30 Ma), continued to some extent until at least the late Oligocene (~25 Ma) and terminated before 18 Ma. This conclusion is in agreement with the proposed late Paleogene age for rotations, which have been observed farther north, in the Antofagasta region [*Somoza et al.*, 1999; *Arriagada et al.*, 2000, 2003].

8. Discussion: Origin of the Rotation Pattern

[56] *Isacks* [1988] suggested that an along-strike variation in the magnitude of Neogene crustal shortening in Bolivia and northwestern Argentina has increased the seaward concavity of the continental margin. This model predicts a wholesale 10–15° counterclockwise rotation of the Peruvian forearc and 5–10° clockwise rotations for most of northern Chile during the Neogene. Although Isacks' model was the first in which variations in horizontal shortening in the Sub-Andean zone were related to Neogene rotation of the forearc, it doesn't explain the larger counterclockwise rotations found in older rocks of southern Peru or the large clockwise rotations observed in Paleogene and oldest rocks in northern Chile. *Beck* [1988] explained clockwise rotations in northern Chile and counterclockwise rotations in southern Peru as the result of distributed crustal shear in the forearc as a consequence of oblique plate convergence. Others authors referring to our studied region, have suggested "domino style" rotations of blocks bounded by oblique NW left-lateral faults between N-S fault strands of the Atacama Fault System [*Forsythe and Chisholm*, 1994; *Taylor et al.*, 1998]. *Taylor et al.* [1998] suggested that, the Coastal Cordillera was rotated during the mid-Cretaceous, as a consequence of domino style deformation on NW trending, fault-bounded blocks inside a large-scale left-lateral strike-slip duplex, enclosed between N-S regional faults, to be found offshore, and along the eastern border of the Coastal Cordillera "Central Valley Shear Zone" [*Randall et al.*, 1996]. While *Abels and Bischoff* [1999] consider rotation between NW trending left-lateral wrench faults which transect the whole north Chilean forearc, *Taylor et al.* [2005] suggest that the obliquity of convergence, coupled with these preexisting NW to NNW structures, was the driving mechanism for the origin of the regional rotation pattern.

[57] However, the occurrence of large sinistral displacements along NW faults is not consistent with the ground truth provided by the inspection of the detailed geological maps now available for most of the southern Atacama region [*Naranjo and Puig*, 1984; *Cornejo et al.*, 1993, 1998; *Arévalo*, 1994; *Cornejo and Mpodozis*, 1996; *Marinovic et al.*, 1995; *Iriarte et al.*, 1996; *Godoy and Lara*, 1998; *Matthews et al.*, 2006]. These considerations led us to propose that the wide-scale rotation field of northern Chile cannot be explained only as a consequence of domino-style fault models or local tectonics within specific, but regionally restricted, tectonic domains. A common mechanism to generate the large-scale rotation pattern is needed in conjunction with effects associated to localized structures. Rotation variability in the Precordillera may be related to thermal crustal weakening by arc magmas during the Eocene Incaic event [*Cornejo et al.*, 1993; *Tomlinson et al.*, 1993]. *Randall et al.* [2001] showed that this event permitted the formation of small-sized rigid tectonic blocks, which rotated independently along a 40 km wide longitudinal belt centered in the Domeyko Fault System [*Mpodozis et al.*, 1993; *Randall et al.*, 2001] (Figures 8, 9, and 10). In any case, this pattern appears to be a subordinate effect superimposed over the much larger-scale paleomagnetic rotation field of the central Andes.

[58] *Roperch et al.* [2006] found large counterclockwise rotations in Eocene-Oligocene sediments along the southern Peruvian forearc. As with the data from the Chilean forearc, there is no evidence for significant Miocene rotation along the forearc of southern Peru. These authors suggest that the counterclockwise rotations in the forearc are the consequence of deformation within the Abancay deflection of the Eastern Cordillera [*Perelló et al.*, 2003]. We propose that clockwise rotations in northern Chile were simultaneous with counterclockwise rotations in southern Peru. Do the large clockwise rotations in Chile also reflect the initial stages of oroclinal bending? According to *Isacks* [1988], oroclinal bending implies that shortening accommodates rotations. Where are the structures accommodating the postulated late Paleogene shortening in the southern central Andes? As in Peru, deformation within the forearc is not enough to accommodate large rotations, structures such as the Potrerillos Fold and Thrust Belt accommodate only a small amount of horizontal shortening, probably less than 20 km [*Tomlinson et al.*, 1993]. Farther north and south, the thick skinned tectonic style with high-angle reverse faults involving the Paleozoic basement which characterizes the deformation of the Precordillera and Cordillera Frontal also indicate a likely low amount of shortening [*Moscoso and Mpodozis*, 1988; *Mpodozis et al.*, 1993]. During the Eocene, oblique subduction might have induced dextral shear in the forearc. However, dextral shear has been documented only for a few minor NE faults segments at the southern termination of the Potrerillos Fold and Thrust Belt [*Randall et al.*, 2001, Figure 2]. In contrast, sinistral shear during the Eocene along the major faults strands of Domeyko Fault System, in the Precordillera, have been described by various authors [*Mpodozis et al.*, 1993; *Tomlinson et al.*, 1993; *Niemeyer*, 1999].

[59] Farther east, detailed studies in the Bolivian Eastern Cordillera have provided evidences for large amounts of shortening. Fission track data, detailed chronostratigraphic analysis and structural studies [*Coutand et al.*, 2001; *Müller et al.*, 2002; *Elger et al.*, 2005; *Haschke et al.*, 2005; *Horton*, 2005; *McQuarrie et al.*, 2005] suggest that uplift and deformation started in the Eocene by eastward directed

thrusting to be followed by west facing "backthrusting" in the central and western Eastern Cordillera during the Oligocene to early Miocene [*McQuarrie and DeCelles*, 2001; *Müller et al.*, 2002]. Long lived shortening from 40 to 15 Ma may have thickened the crust and uplifted the Eastern Cordillera [*Benjamin et al.*, 1987; *Masek et al.*, 1994; *Lamb*, 2001] where deformation essentially ceased by 10 Ma [*Gubbels et al.*, 1993]. The beginning of deformation within the Chilean Precordillera was contemporaneous with the onset of deformation of the Eastern Cordillera. *McQuarrie and DeCelles* [2001] and *McQuarrie et al.* [2005] proposed eastward propagation of a 200–400 km long, 15 km thick, basement megathrust sheet rooted in the "Western Cordillera". Although this hypothesis is debatable, it is one of the first attempts to link Eocene-Oligocene deformation in the Eastern Cordillera with coeval tectonics within the magmatic arc in Chile (at that time located in the Chilean Precordillera or Cordillera de Domeyko, not in the Western Cordillera).

[60] To understand the rotation field found between 22 and 28°S both large-scale, orogen-wide effects and rotations related to local deformation need to be assessed jointly. In recent years it has become clear that crustal shortening alone appears insufficient to explain the large along strike variations in cross sectional Andean volume [*Allmendinger et al.*, 1997; *Kley and Monaldi*, 1998] which appears to require, besides magmatic underplating and lithospheric thinning by delamination, important mass transfer by lateral crustal flow [*Dewey and Lamb*, 1992; *Husson and Sempere*, 2003; *Yang et al.*, 2003]. If we consider all data presently available, the Eocene-Oligocene tectonic regime in the central Andes can be well described in terms of *Lamb*'s [1994] "floating block model" as an array of rotating rigid upper crustal blocks, floating over a ductile lower crust flowing in direction to a zone of crustal weakness, located in the Eastern Cordillera [*Lamb*, 2001; *Kley et al.*, 2005].

[61] Up to 10 km of mostly Ordovician sandstone and shale accumulated on a highly attenuated early Paleozoic rift basin in the Eastern Cordillera failed under regional compression during the Eocene-Oligocene [*Jaillard et al.*, 2000; *Müller et al.*, 2002; *McQuarrie et al.*, 2005]. Large-scale but localized horizontal shortening may have been equilibrated in the hinterland by rigid block rotations and enhanced crustal flow toward the Eastern Cordillera from both flanks of the Orocline.

[62] Paleomagnetically determined rotations in middle Miocene and younger rocks are much smaller than the rotations determined for older rocks (Figure 10). Middle Miocene to Recent deformation, which occurred under conditions of nearly orthogonal plate convergence [*Pardo-Casas and Molnar*, 1987; *Somoza*, 1998], corresponds mainly to east-west shortening with only a small component of margin-parallel displacements, favoring Andean uplift and growth after the end of an Eocene to early Miocene period with significant rotations. Eocene–early Miocene deformation, which occurred during a period of highly oblique plate convergence, may have included an important component of trench-parallel mass transfer toward the Arica Bend more important than the one proposed by *Hindle et al.* [2005] for the late Neogene.

9. Conclusions

[63] 1. We have obtained paleomagnetic results for 133 paleomagnetic sites along the northern Chile forearc region between 25°S and 28°S. Magnetization in volcanic and intrusive rocks is primary and was acquired upon cooling. Several sites in sediments have been remagnetized. The pretectonic or posttectonic nature of the magnetization was assessed through fold tests at the locality level. Tilt correction decreases the dispersion of the mean-site directions at nine localities while syntectonic and posttectonic magnetizations were observed at two and four localities, respectively. We interpret the remagnetization in the Central Depression, Precordillera and Frontal Cordillera as a result of local heating and/or fluid flow during Paleogene magmatic arc activity.

[64] 2. The north Chilean forearc between 22° and 28°S presents clockwise rotations up to 35° to 40° at most localities. Block rotations are recorded in Jurassic to Oligocene rocks. Paleomagnetic results in the circa 18 Ma Río Frío Ignimbrite covering rotated and nonrotated blocks confirm a pre-early Miocene age of the relative rotations within the study area. Our new data provide evidence that rotations occurred essentially during the Eocene–early Oligocene (40–30 Ma) continued to until at least the late Oligocene (~25 Ma) but essentially terminated before 18 Ma. Overall, the magnitude of rotation is similar both in the Coastal Cordillera and Central Depression domains. An orogen-scale mechanism combined with localized tectonics controlling the rotation of small-sized blocks within the thermally weakened crust of the Eocene magmatic arc (Precordillera) is needed to explain the observed rotation field. Yet, the large-scale regional pattern of rotation cannot be explained by Precordilleran deformation only. Deformation and block rotations within the forearc are not simply the consequence of strain controlled by trench-linked strike-slip faults during oblique convergence.

[65] 3. Deformation of the Precordillera and clockwise block rotations in the forearc of northern Chile are simultaneous with counterclockwise rotations of the forearc of southern Peru [*Roperch et al.*, 2006]. The central Andes rotation pattern seems to be closely related and mechanically linked to processes of Eocene-Oligocene differential horizontal shortening focused in the Eastern Cordillera of Bolivia. Eastern Cordillera shortening may have been balanced by southeast directed (southern Peru) and northeast directed (northern Chile) crustal flow and transfer of mass toward the Eastern Cordillera, which ultimately led to the formation of the Bolivian Orocline during the Paleogene.

[66] **Acknowledgments.** Financial support for this project was provided by the Institut de Recherche pour le Développement (IRD) and FONDECYT-Chile (grants 1970002, 3030050, and 1050750). Guillaume Dupont-Nivet and Pierre Gautier participated in one of the field trips. We especially thank Guillaume for making several measure-

ments in the early stages of this study. Comments from referees Graeme Taylor, Stuart Gilder, and Gabriel González helped reorganize and clarify the content of the paper. Discussions with Andy Tomlinson, Paula Cornejo, Peter Cobbold, and Rubén Somoza were very helpful. We would also like to thank Sergio Villagrán (IRD, Santiago) for assistance in the field.

References

Abels, A., and L. Bischoff (1999), Clockwise block rotations in northern Chile: Indicators for a large-scale domino mechanism during the middle-late Eocene, *Geology*, *27*, 751–754.

Allmendinger, R. W., T. E. Jordan, S. M. Kay, and B. L. Isacks (1997), The evolution of the Altiplano-Puna Plateau of the central Andes, *Annu. Rev. Earth Planetary Sci.*, *25*, 139–174.

Arévalo, C. (1994), Mapa Geológico de la Hoja Los Loros, *Doc. Trabajo 6*, scale 1:100,0000, Serv. Nac. Geol. y Min., Santiago.

Arévalo, C. (1999), The Coastal Cordillera/Precordillera boundary in the Tierra Amarilla area (27°20′–27°40′S/70°05–70°20′W), northern Chile, and the structural setting of the Candelaria Cu-Au ore deposit, Ph.D. thesis, 294 pp., Kingston Univ., Kingston, U. K.

Arévalo, C., O. Rivera, S. Iriarte, and C. Mpodozis (1994), Cuencas extensionales y campos de calderas del Cretácico Superior-Terciario Inferior en la Precordillera de Copiapó (27–28°S), Chile, paper presented at 7th Chilean Geological Congress, Univ. Concepción., Concepción, Chile.

Arriagada, C., P. Roperch, and C. Mpodozis (2000), Clockwise block rotations along the eastern border of the Cordillera de Domeyko, northern Chile (22°45′–23°30′S), *Tectonophysics*, *326*, 153–171.

Arriagada, C., P. Roperch, C. Mpodozis, G. Dupont-Nivet, P. R. Cobbold, A. Chauvin, and J. Cortés (2003), Paleogene clockwise tectonic rotations in the forearc of central Andes, Antofagasta region, northern Chile, *J. Geophys. Res.*, *108*(B1), 2032, doi:10.1029/2001JB001598.

Aubry, L., P. Roperch, M. de Urreiztieta, E. Rosello, and A. Chauvin (1996), Paleomagnetic study along the southeastern edge of the Altiplano–Puna Plateau: Neogene tectonic rotations, *J. Geophys. Res.*, *101*, 17,883–17,899.

Beck, M. E. (1988), Analysis of Late Jurassic-Recent paleomagnetic data from active plate margins of South America, *J. S. Am. Earth Sci.*, *1*, 39–52.

Benjamin, M., N. Johnson, and C. Naeser (1987), Recent rapid uplift in the Bolivian Andes: Evidence from fission-track dating, *Geology*, *15*, 680–683.

Besse, J., and V. Courtillot (2002), Apparent and true polar wander and the geometry of the geomagnetic field over the last 200 Myr, *J. Geophys. Res.*, *107*(B11), 2300, doi:10.1029/2000JB000050.

Butler, R. F., D. R. Richards, T. Sempere, and L. G. Marshall (1995), Paleomagnetic determinations of vertical-axis tectonic rotations from Late Cretaceous and Paleocene strata of Bolivia, *Geology*, *23*, 799–802.

Cahill, T., and B. L. Isacks (1992), Seismicity and shape of the subducted Nazca Plate, *J. Geophys. Res.*, *97*, 17,503–17,529.

Cogné, J. P. (2003), PaleoMac: A Macintosh® application for treating paleomagnetic data and making plate reconstructions, *Geochem. Geophys. Geosyst.*, *4(1), 1007, doi:10.1029/2001GC000227.*

Cornejo, P., and S. Matthews (2000), Relación entre magmatismo-tectonica y su implicancia en la formación de sistemas de pórfidos cupriferos: Yacimiento El Salvador, III Región, Chile, paper presented at VIII Congreso Geológico Chileno, Serv. Nac de Geol y Min., Puerto Varas, Chile.

Cornejo, P., and C. Mpodozis (1996), Geología de la Región de Sierra Exploradora (25°–26° Lat. S), *Reg. Rep. IR-96-09*, 2 vols., 8 maps, scale 1:50,000, Serv. Nac. de Geol. y Min., Santiago.

Cornejo, P., C. Mpodozis, C. Ramírez, and A. Tomlinson (1993), Estudio geológico de la Región de Potrerillos y El Salvador (26°–27° Lat. S), *Reg. Rep. IR-93-01*, 2 vols., 12 maps, scale 1:50,000, Serv. Nac. de Geol. y Min., Santiago.

Cornejo, P., C. Mpodozis, and A. J. Tomlinson (1998), Hoja Salar de Maricunga, Región de Atacama, *Mapas Geol*, *7*, scale 1:10,0000, Serv. Nac. de Geol. y Min., Santiago.

Cornejo, P., C. Mpodozis, and S. Matthews (1999), Geología y evolución magmática del distrito Indio Muerto y Yacimiento El Salvador, *Reg. Rep. IR 98-14*, 1–99 pp., 1 map, scale 1:25,000, Serv. Nac. de Geol. y Min., Santiago.

Coutand, I., P. Roperch, A. Chauvin, P. R. Cobbold, and P. Gautier (1999), Vertical axis rotations across the Puna plateau (northwestern Argentina) from paleomagnetic analysis of Cretaceous and Cenozoic rocks, *J. Geophys. Res.*, *104*, 22,965–22,984.

Coutand, I., P. R. Cobbold, M. de Urreiztieta, P. Gautier, A. Chauvin, D. Gapais, E. A. Rossello, and O. López-Gamundí (2001), Style and history of Andean deformation, Puna plateau, northwestern Argentina, *Tectonics*, *20*, 210–234.

Dallmeyer, R. D., M. Brown, J. Grocott, G. K. Taylor, and P. J. Treloar (1996), Mesozoic magmatic and tectonic events within the Andean plate boundary zone, 26°–27°30′S, north Chile: Constraints from $^{40}Ar/^{39}Ar$ mineral ages, *J. Geol.*, *104*, 19–40.

Demarest, H. (1983), Error analysis for the determination of tectonic rotation from paleomagnetic data, *J. Geophys. Res.*, *88*, 4321–4328.

Dewey, J. F., and S. H. Lamb (1992), Active tectonics of the Andes, *Tectonophysics*, *205*, 79–95.

Elger, K., O. Oncken, and J. Glodny (2005), Plateau style accumulation of deformation: southern Altiplano, *Tectonics*, *24*, TC4020, doi:10.1029/2004TC001675.

Fernández, R. (2003), Paleomagnetismo y tectónica en la Cordillera de Domeyko entre los 26°00′ y 27°15′ Latitud Sur, Region de Atacama, Chile, M.Sc. thesis, 134 pp., Univ. de Chile, Santiago.

Forsythe, R., and L. Chisholm (1994), Paleomagnetic and structural constraints on rotations in the north Chilean Coast Ranges, *J. S. Am. Earth Sci.*, *7*, 279–294.

Godoy, E., and L. Lara (1998), Hojas Chañaral y Diego de Almagro, *Mapas Geol. 5–6*, scale 1:100,000, Serv. Nac. Geol. y Min., Santiago.

Grocott, J., and G. Taylor (2002), Magmatic arc fault systems, deformation partitioning and emplacement of granitic complexes in the Coastal Cordillera, north Chilean Andes (25°30′S to 27°00′S), *J. Geol. Soc. London*, *159*, 425–442.

Gubbels, T., B. Isacks, and E. Farrar (1993), High-level surfaces, plateau uplift, and foreland development, Bolivian central Andes, *Geology*, *21*, 695–698.

Haschke, M., A. Deeken, N. Insel, E. Sobel, M. Grove, and A. K. Shmitt (2005), Growth pattern of the Andean Puna plateau constrained by apatite fission track, apatite (U-Th)/He, K-feldspar $^{40}Ar/^{39}Ar$, and zircon U-Pb geochronology, in *Andean Geodynamics*, *6th International Symposium, Barcelona, Spain Sept. 2005*, pp. 360–363, Inst. de Rech. pour le Dév., Paris.

Hindle, D., J. Kley, O. Oncken, and S. Sobolev (2005), Crustal balance and crustal flux from shortening estimates in the central Andes, *Earth Planet. Sci. Lett.*, *230*, 113–124.

Horton, B. K. (2005), Revised deformation history of the central Andes: Inferences from Cenozoic foredeep and intermontane basins of the Eastern Cordillera, Bolivia, *Tectonics*, *24*, TC3011, doi:10.1029/2003TC001619.

Husson, L., and T. Sempere (2003), Thickening the Altiplano crust by gravity-driven crustal channel flow, *Geophys. Res. Lett.*, *30*(5), 1243, doi:10.1029/2002GL016877.

Iriarte, S., C. Arévalo, C. Mpodozis, and O. Rivera (1996), Mapa Geológico de la Hoja Carrera Pinto, *Mapas Geol. 3*, scale 1:100,000, Serv. Nac. Geol. y Min., Santiago.

Isacks, B. L. (1988), Uplift of the central Andean plateau and bending of the Bolivian orocline, *J. Geophys. Res.*, *93*, 3211–3231.

Jaillard, E., G. Hérail, T. Monfret, E. Díaz Martínez, P. Baby, A. Lavenu, and J. F. Dumont (2000), Tectonic evolution of the Andes of Ecuador, Peru, Bolivia, and northernmost Chile, in *Tectonic Evolution of South America*, edited by U. Cordani et al., pp. 481–559, Fundo Setorial de Pet. e Gás Nat., Rio de Janeiro, Brazil.

Kay, S. M., C. Mpodozis, V. Ramos, and F. Munizaga (1991), Magma source variations for mid Late Tertiary magmatic rocks associated with a shallowing subduction zone and a thickened crust in the central Andes (28° to 33°S), *Spec. Pap., Geol. Soc. Am.*, *265*, 113–137.

Kirschvink, J. L. (1980), The least-squares line and plane and the analysis of paleomagnetic data, *Geophys. J. R. Astron. Soc.*, *62*, 699–718.

Kley, J., and C. R. Monaldi (1998), Tectonic shortening and crustal thickness in the central Andes: How good is the correlation?, *Geology*, *26*, 723–726.

Kley, J., C. R. Monaldi, E. Rossello, and H. Ege (2005), The Eastern Cordillera of the Central Andes: Inherited mechanical weakness as a first-order control on the Cenozoic orogeny, in *Andean Geodynamics*, *6th International Symposium*, *Barcelona, Spain, Sept. 2005*, pp. 432–435, Inst. de Rech. pour le Dév., Paris.

Lamb, S. (1994), Behavior of the brittle crust in wide plate boundary zones, *J. Geophys. Res.*, *99*, 4457–4483.

Lamb, S. (2001), Vertical axis rotation in the Bolivian orocline, South America: 1. Paleomagnetic analysis of Cretaceous and Cenozoic rocks, *J. Geophys. Res.*, *106*, 26,605–26,632.

Lamb, S. H., and D. E. Randall (2001), Deriving palaeomagnetic poles from independently assesed inclination and declination data: Implications for South American poles since 120 Ma, *Geophys. J. Int.*, *146*, 349–370.

Macedo Sanchez, O., J. Surmont, C. Kissel, and C. Laj (1992), New temporal constraints on the rotation of the Peruvian central Andes obtained from paleomagnetism, *Geophys. Res. Lett.*, *19*, 1875–1878.

MacFadden, B. J., F. Anaya, and C. C. Swisher III (1995), Neogene paleomagnetism and oroclinal bending of the central Andes of Bolivia, *J. Geophys. Res.*, *100*, 8153–8167.

Maksaev, V., and M. Zentilli (1999), Fission track: Thermochronology of the Domeyko Cordillera, northern Chile: Implications for Andean tectonics and porphyry cooper metallogenesis, *Explor. Min. Geol.*, *8*, 65–89.

Marinovic, N., I. Smoje, M. Hervé, and C. Mpodozis (1995), Hoja Aguas Blancas, *Carta Geol. Chile 70*, scale 1:250,000, pp. 1–150, Serv. Nac. Geol. y Min., Santiago.

Marsh, T., M. Einaudi, and M. McWilliams (1997), $^{40}Ar/^{39}Ar$ geochronology of Cu-Au and Au-Ag mineralization in the Potrerillos District, Chile, *Econ. Geol.*, *92*, 784–806.

Masek, J. G., B. L. Isacks, and E. J. Fielding (1994), Erosion and tectonics at the margins of continental plateaus, *J. Geophys. Res.*, *99*, 13,941–13,956.

Matthews, S., P. Cornejo, and R. Riquelme (2006), Hoja Inca de Oro, *Carta Geol. Chile*, 1:100,000

scale, Serv. Nac. Geol. y Min., Santiago, in press.

McFadden, P. L., and M. W. McElhinny (1988), The combined analysis of remagnetization circles and direct observations in paleomagnetism, *Earth Planet. Sci. Lett.*, *87*, 161–172.

McQuarrie, N., and P. DeCelles (2001), Geometry and structural evolution of the central Andean back thrust belt, Bolivia, *Tectonics*, *20*, 669–692.

McQuarrie, N., B. Horton, G. Zandt, S. Beck, and P. DeCelles (2005), Lithospheric evolution of the Andean fold-thrust belt, Bolivia, and the origin of the central Andean plateau, *Tectonophysics*, *399*, 15–37.

Moscoso, R., and C. Mpodozis (1988), Estilos estructurales en el Norte Chico de Chile, *Rev. Geol. Chile*, *15*, 151–166.

Mpodozis, C., and R. W. Allmendinger (1993), Extensional tectonics, Cretaceous Andes, northern Chile (278°S), *Geol. Soc. Am. Bull.*, *105*, 1462–1477.

Mpodozis, C., and J. Clavero (2002), Tertiary tectonic evolution of the southwestern edge of the Puna plateau: Cordillera Claudio Gay (26°–27°S), northern Chile, in *Andean Geodynamics, 5th International Symposium, Toulouse, France*, pp. 445–448, Inst. Rech. Dev., Paris.

Mpodozis, C., and V. A. Ramos (1990), The Andes of Chile and Argentina, in *Geology of the Andes and Its Relation to Hydrocarbon and Mineral Resources*, *Earth Sci. Ser.*, vol. 11, pp. 59–90, Circum-Pac. Counc. Energy and Mineral. Resour., Houston, Tex.

Mpodozis, C., N. Marinovic, and I. Smoje (1993), Eocene left lateral strike slip faulting and clockwise block rotations in the Cordillera de Domeyko, west of Salar de Atacama, northern Chile, in *Andean Geodynamics*, *2nd International Symposium*, *Oxford Press, U. K.* pp. 225–228, ORSTOM, Paris.

Mpodozis, C., P. Cornejo, S. M. Kay, and A. Titler (1995), La Franja de Maricunga: Síntesis de la evolución del Frente Volcánico Oligoceno-Mioceno de la zona sur de los Andes Centrales, *Rev. Geol. Chile*, *21*, 273–313.

Mpodozis, C., C. Arriagada, M. Basso, P. Roperch, P. Cobbold, and M. Reich (2005), Mesozoic to Paleogene stratigraphy of the Atacama (Purilactis) Basin, Antofagasta region, northern Chile: Insights into the earlier stages of central Andean tectonic evolution, *Tectonophysics*, *399*, 125–154.

Müller, J. P., J. Kley, and V. Jacobshagen (2002), Structure and Cenozoic kinematics of the Eastern Cordillera, southern Bolivia (21°S), *Tectonics*, *21*(5), 1037, doi:10.1029/2001TC001340.

Muñoz, J. A., A. Amilibia, N. Carrera, G. Mon, G. Chong, E. Roca, and F. A. Sabat (2005), A geological cross section of the Andean orogen at 25.5 LS, in *Andean Geodynamics*, *6th International Symposium*, *Barcelona, Spain, Sept. 2005*, pp. 536–539, Inst. de Rech. pour le Dév., Paris.

Nalpas, T., G. Hérail, R. Mpodozis, J. Clavero, and M. P. Dabard (2005), Thermochronological data and denudation history along a transect between Chañaral and Pedernales (~26°S), north Chilean Andes: Orogenic implications, in *Andean Geodynamics*, *6th International Symposium*, *Barcelona, Spain, Sept. 2005*, pp. 548–551, Inst. de Rech. pour le Dév., Paris.

Naranjo, J. A., and A. Puig (1984), Hojas Taltal y Chañarall, *Carta Geol. Chile 62–63*, scale 1:250,000, 140 pp., Serv. Nac. de Geol. y Min., Santiago.

Niemeyer, H. (1999), Nuevos datos cinemáticos para la Falla Sierra Castillo en Quebrada del Carrizo, Precordillera de la Región de Atacama, Chile, *Rev. Geol. Chile*, *26*, 159–174.

Pardo-Casas, F., and P. Molnar (1987), Relative motion of the Nazca (Farallon) and South American plates since Late Cretaceous times, *Tectonics*, *6*, 233–248.

Perelló, J., V. Carlotto, A. Zárate, P. Ramos, H. Posso, C. Neyra, A. Caballero, N. Fuster, and R. Muhur (2003), Porphyry-style alteration and mineralization of the middle Eocene to early Oligocene Andahuaylas-Yauri Belt, Cuzco region, Peru, *Econ. Geol.*, *98*, 1575–1605.

Randall, D. E. (1998), A new Jurassic-Recent apparent polar wander path for South America and a review of central Andean tectonic models, *Tectonophysics*, *299*, 49–74.

Randall, D. E., G. K. Taylor, and J. Grocott (1996), Major crustal rotations in the Andean margin: Paleomagnetic results from the Coastal Cordillera of northern Chile, *J. Geophys. Res.*, *101*, 15,783–15,798.

Randall, D. E., A. J. Tomlinson, and G. K. Taylor (2001), Paleomagnetically defined rotations from the Precordillera of northern Chile: Evidence of localized in situ fault-controlled rotations, *Tectonics*, *20*, 235–254.

Riley, P. D., M. E. Beck, R. F. Burmester, C. Mpodozis, and A. García (1993), Paleomagnetic evidence of vertical axis block rotations from the Mesozoic of northern Chile, *J. Geophys. Res.*, *98*, 8321–8333.

Roperch, P., and G. Carlier (1992), Paleomagnetism of Mesozoic rocks from the central Andes of southern Peru: Importance of rotations in the development of the Bolivian Orocline, *J. Geophys. Res.*, *97*, 17,233–17,249.

Roperch, P., M. Fornari, G. Hérail, and G. Parraguez (2000), Tectonic rotations within the Bolivian Altiplano: Implications for the geodynamic evolution of the central Andes during the late Tertiary, *J. Geophys. Res.*, *105*, 795–820.

Roperch, P., T. Semperé, O. Macedo, C. Arriagada, M. Fornari, C. Tapia, M. García, and C. Laj (2006), Counterclockwise rotation of late Eocene–Oligocene fore-arc deposits in southern Peru and its significance for oroclinal bending in the central Andes, *Tectonics*, *25*, TC3010, doi:10.1029/2005TC001882.

Servicio Nacional de Geología y Minería (2003), Mapa Geológico de Chile, scale 1:1,000,000, Santiago.

Somoza, R. (1998), Updated Nazca (Farallon)-South America relative motions during the last 40 My: Implications for mountains building in the central Andean region, *J. S. Am. Earth Sci.*, *11*, 211–215.

Somoza, R., and A. Tomlinson (2002), Paleomagnetism in the Precordillera of northern Chile (22°30′S): Implications for the history of tectonic rotations in the central Andes, *Earth Planet. Sci. Lett.*, *194*, 369–381.

Somoza, R., S. Singer, and A. Tomlinson (1999), Paleomagnetic study of upper Miocene rocks from northern Chile: Implications for the origin of late Miocene–Recent tectonic rotations in the southern central Andes, *J. Geophys. Res.*, *104*, 22,923–22,936.

Taylor, G., J. Grocott, A. Pope, and D. Randall (1998), Mesozoic fault systems, deformation and fault block rotation in the Andean forearc: A crustal scale strike-slip duplex in the Coastal Cordillera of northern Chile, *Tectonophysics*, *299*, 93–109.

Taylor, G., M. Gipson, and J. Groccot (2002), New palaeomagnetic results from the Coastal Cordillera/Precordillera boundary northern Chile: Implications for plate margin deformation, in *Andean Geodynamics*, *5th International Symposium*, *Toulouse, France*, 633–636, Inst. de Rech. Pour le Dév., Paris.

Taylor, G., B. Dashwood, and J. Groccot (2005), Central Andean rotation patter: Evidence from paleomagntic rotations of an anomalous domain in the forearc of northern Chile, *Geology*, *33*, 777–780.

Tomlinson, A., C. Mpodozis, P. Cornejo, and C. Ramirez (1993), Structural geology of the Sierra Castillo-Agua Amarga Fault System, Precordillera of Chile, El Salvador-Potrerillos, in *Andean Geodynamics*, *2nd International Symposium*, *Oxford Press, U. K.*, pp. 259–262, ORSTOM, Paris.

Tomlinson, A., P. Cornejo, and C. Mpodozis (1999), Hoja Potrerillos, Región de Atacama, *Mapas Geol.*, *14, scale 1:100,000, Serv. Nac. de Geol. y Min, Santiago.*

Yang, Y., M. Liu, and S. Stein (2003), A 3-D geodynamic model of lateral crustal flow during Andean mountain building, *Geophys. Res. Lett.*, *30*(21), 2093, doi:10.1029/2003GL018308.

C. Arriagada and R. Fernandez, Departamento de Geología, Universidad de Chile, Plaza Ercilla 803, Santiago, Chile. (cearriag@cec.uchile.cl)

C. Mpodozis, ENAP-Sipetrol, Avenida Vitacura 2736, Santiago, Chile. (cmpodozis@sipetrol.cl)

P. Roperch, IRD, UR154 and Géosciences Rennes, Université de Rennes 1, Campus de Beaulieu, CS 74205, F-35042, Rennes Cedex, France. (pierrick.roperch@ird.fr)